iScience

CellPress
OPEN ACCESS

Article

A safer cell-based yellow fever live attenuated vaccine protects mice against YFV infection

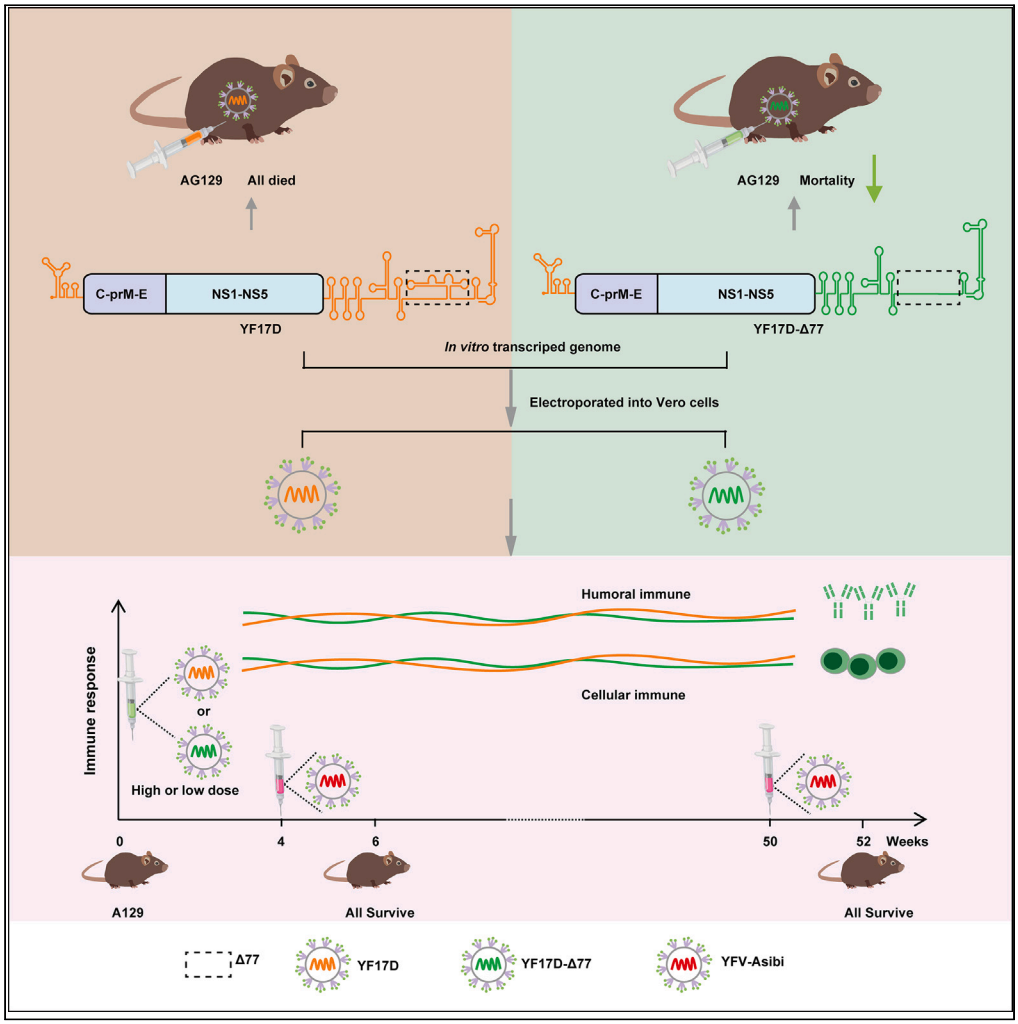

Weiwei Guo, Tingting Jiang, Juhong Rao, ..., Mingqing Lu, Xue Hu, Chao Shan

shanchao@wh.iov.cn

Highlights

Deletions in the 3′UTR of the YF17D genome led to further attenuation of the virus

A single dose of YF17D-Δ77 provides complete and long-lasting immune protection

YF7D-Δ77 exhibits equivalent immunogenicity and efficacy in mice

YF17D-Δ77 showed strong genetic stability after 20-round passage in cell culture

Guo et al., iScience 27, 110972
October 18, 2024
https://doi.org/10.1016/j.isci.2024.110972

iScience

CellPress
OPEN ACCESS

Article

A safer cell-based yellow fever live attenuated vaccine protects mice against YFV infection

Weiwei Guo,[1,2,4] Tingting Jiang,[1,2,3] Juhong Rao,[1,2,4] Zihan Zhang,[1,2,4] Xuekai Zhang,[1,2,4] Jiaoling Su,[1,2,4] Chunhong Yin,[1,2,3] Mingqing Lu,[1,2,4] Xue Hu,[1,2,3] and Chao Shan[1,2,3,4,5,6,*]

SUMMARY

The live attenuated yellow fever vaccine (YF17D) has caused controversial safety issues in history with low-yield problems, which has led to a large population being unable to be vaccinated and vaccine shortage in facing recent outbreaks. Here, we report a safer live attenuated vaccine candidate, YF17D-Δ77, which contains 77 nucleotides deletion in the 3′ untranslated region (3′ UTR) of the YF17D genome. YF17D-Δ77 exhibited no neurotropism and decreased viscerotropism and caused significantly lower lethality in mice compared to YF17D. Mechanistically, the deletion enhanced the sensitivity of the virus to type I and type II interferon responses, which hindered viral replication. Encouragingly, YF17D-Δ77 provided comparable immune protection in mice as did YF17D. Even 10 PFU of YF17D-Δ77 completely protected mice against YFV-Asibi challenge. In addition, the Δ77 mutation showed excellent stability after successive passages in Vero cells. Collectively, the data suggest that further development of YF17D-Δ77 as vaccine candidate is warranted.

INTRODUCTION

Yellow fever virus (YFV), the prototype member of the genus *Flavivirus*, shares similar biological characteristics with other highly pathogenic members of the genus, such as Dengue virus (DENV), Zika virus (ZIKV), Japanese encephalitis virus (JEV), and West Nile virus (WNV), all of which have an envelope structure encasing a positive-sense RNA genome of approximately 11,000 nucleotides.[1–3] The viral genome encodes a single open reading frame (ORF) flanked by highly structured 5′- and 3′-untranslated regions (UTRs).[4] YFV is the etiologic agent of yellow fever (YF), which is endemic to 47 countries in tropical America and Africa.[5,6] Annually, there are approximately 200,000 YF cases and more than 50,000 fatalities worldwide.[7,8] YF is a viscerotropic disease characterized by multiorgan dysfunction and hemorrhagic fever.[3,9] There are currently no specific antiviral treatments available. YFV is transmitted to humans by *Haemagogus*, *Sabethes* and *Aedes* mosquitoes.[3] The epidemic of YF has largely been controlled by the deployment of a live attenuated vaccine, YF17D, one of the most effective viral vaccines since it was first used in 1937.[10–12] Nonetheless, the sylvatic circulation of YFV between mosquitoes and nonhuman primates (NHPs) has resulted in occurrences of intense YF reemergence event.[8,13–15] Moreover, owing to its nature as a live attenuated vaccine, the safety of YF17D has caused some controversy because of the presence of rare vaccine-related severe adverse events, including YF vaccine-associated neurotropic disease (YEL-AND) and YF vaccine-associated viscerotropic disease (YEL-AVD), with a morbidity of 0.8/100,000 and 0.4/100,000, respectively.[3,16–18] Thus, the World Health Organization (WHO) constrains or precludes vaccination with YF17D in some groups, including infants under 9 months of age, elderly individuals over 60 years old, pregnant and lactating women, and immunocompromised individuals,[19] as these individuals are at higher risk of developing YEL-AND and YEL-AVD after vaccination.[17,20] In addition, people with egg allergies are also excluded from vaccination, as the vaccine must be produced in specific pathogen-free embryonated chicken eggs.[10,18] Special manufacturing processes have led to limited vaccine production, which has further led to a shortage of the vaccine in recent massive outbreaks.[21–24] Importantly, outbreaks in 2016–2019 occurred in nonendemic areas and areas with low YFV activity as well as low vaccination coverage.[22,25] The expansion of endemic areas and the frequent recurrence of YF overlap the low yield of the vaccine, which, together with the safety concerns discussed above, emphasize the urgent need to increase the global supply of efficient and safer vaccines. One available strategy to address this issue is to develop new vaccine candidates.

Previous studies have shown that the 3′ UTR of the arthropod-borne flavivirus genome performs multiple functions involved in virus replication,[26–28] virus evolution (transmission and host adaptation),[29–31] evasion of the innate immune response,[32] and viral pathogenicity.[33–35] The 3′ UTR of YFV, similar to those of other arthropod-borne flaviviruses, folds into a conserved secondary structure[29] that has been divided into

[1]Key Laboratory of Virology and Biosafety, Wuhan Institute of Virology, Chinese Academy of Sciences, Wuhan 430071, China
[2]State Key Laboratory of Virology, Wuhan Institute of Virology, Chinese Academy of Sciences, Wuhan 430071, China
[3]Center for Biosafety Mega-Science, Wuhan Institute of Virology, Chinese Academy of Sciences, Wuhan 430071, China
[4]University of the Chinese Academy of Sciences, Beijing 100039, China
[5]Hubei Jiangxia Laboratory, Wuhan 430200, China
[6]Lead contact
*Correspondence: shanchao@wh.iov.cn
https://doi.org/10.1016/j.isci.2024.110972

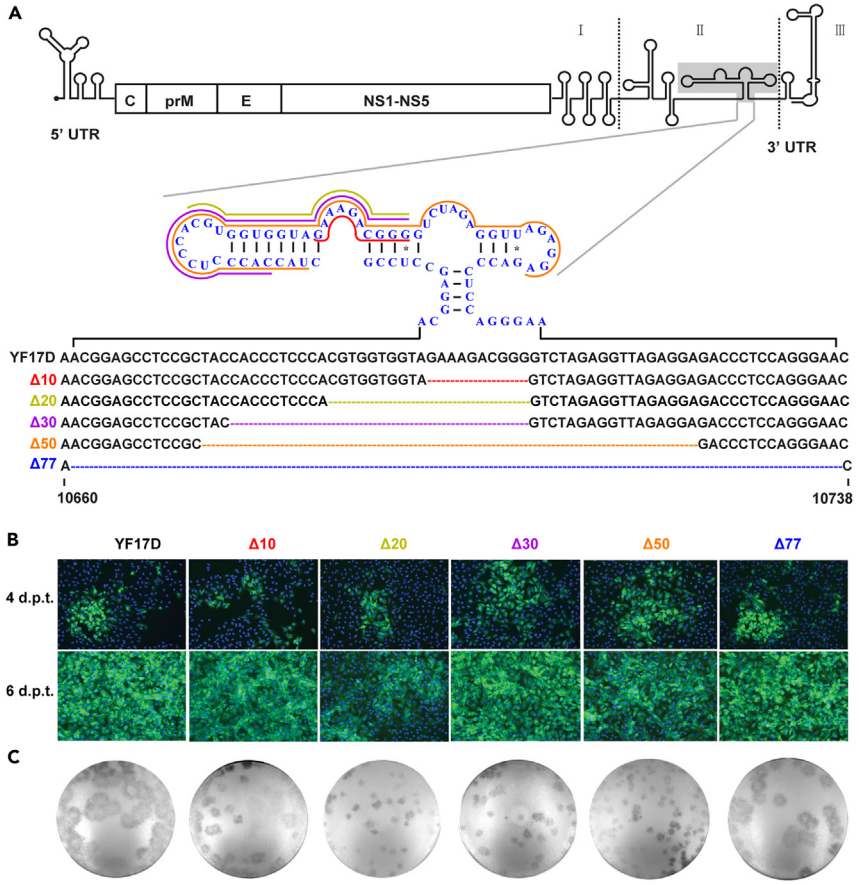

Figure 1. Vaccine design and rescue of YF17D and mutant viruses

(A) Schematic diagram of the YF17D genome and the predicted 3′ UTR structure. The dumbbell structure is located in domain II of the 3′ UTR,[38] and the deleted sequences are color coded (red for Δ10, yellow-green for Δ20, purple for Δ30, orange for Δ50 and blue for Δ77) in the secondary structure and linear genome.

(B) Indirect immunofluorescence assay (IFA) results of YFV E protein expression in Vero cells transfected with *in vitro*-transcribed intact or defective YF17D genome. Ten micrograms of *in vitro*-transcribed intact or defective genome RNA were transfected into Vero cells, and IFA was conducted on days 4 and 6 post-transfection to detect the YF17D E protein. Green fluorescence represents E protein positive cells.

(C) Infection foci of YF17D or mutant viruses in Vero cells. The culture fluids shown in Figure 1B were harvested at 8–10 days post-transfection (P0 viruses) and titrated by an immunostaining focus assay using the 4G2 antibody. d.p.t.: days post-transfection.

three regions: domain I is variable and contains repeated hairpin motifs[36]; domain II is moderately conserved and consists of a characteristic dumbbell (DB)-like structure and CS2 motif present in all mosquito-borne flaviviruses; and domain III is highly conserved, containing cyclization sequences and a stable 3' stem–loop that are essential for viral replication.[37,38] One or two DBs within domain II of mosquito-borne flavivirus have been predicted to form pseudoknot that may prevent complete degradation of the viral genome by the host 5′-3′ exonuclease XRN1 and result in the production of functional subgenomic flavivirus RNA (sfRNA).[4,39,40] The YFV 3′ UTR was predicted to be related to virulence[35]; however, to date, there are no *in vivo* evidence to support this hypothesis but some *in vitro* clues: a significant delay in the emergence of a cytopathic effect (CPE) has been observed in mammalian cells infected by YF17D mutants that are unable to produce sfRNA,[41] and the absence of CS2 resulted in reduced YF17D replication efficiency.[42]

Several successful live attenuated *Flavivirus* vaccines, including DENV4-Δ30[43,44], 10del-ZIKV,[45] and WNV-poly (A),[46] were generated by modifying the 3′ UTR of the respective genome. Notably, both DENV4-Δ30 and 10del-ZIKV were attenuated by deleting partial sequences of the DB region in the 3′ UTR.[43,45] In this study, we report that the DB region within the YF17D 3′ UTR is correlated with viral pathogenicity, and a safer live attenuated YF vaccine candidate was generated by deleting the DB domain based on the backbone of a full-length YF17D (strain 17D RKI, GenBank accession no. JN628279) infectious cDNA clone.

RESULTS

Mutant viruses with deletions in the DB region of the YF17D 3′ UTR are attenuated *in vitro*

The highly structured YF17D 3′ UTR is divided into three regions, with the DB structure located in the moderately conserved domain II (Figure 1A).[38] Drawing on the successful experience of the development of DENV and ZIKV live attenuated vaccine,[33,45] we designed a set of

overlap deletions (Δ10, Δ20, Δ30, Δ50, and Δ77) in the DB region based on an infectious cDNA clone of YF17D. The DB structure was completely removed for YF17D-Δ77 (Figure 1A). The recombinant viruses were recovered via the conventional transfection method. Vero cells transfected with *in vitro*-transcribed defective YF17D genomes (containing deletions in the 3′UTR) were able to express YFV-specific E protein, and the expression of the E protein showed an increasing trend over time (Figure 1B). Mutant viruses of the P0 generation were obtained by harvesting the supernatants of transfected cells at 8–10 days post-transfection (d.p.t.) and were titrated in BHK-21 cells. The titers of the P0 generation Δ10 and Δ77 viruses (7–9×10^6 PFU/mL) were slightly lower than that of YF17D (2 × 10^7 PFU/mL), while the titers of the other three mutant viruses (Δ20, Δ30 and Δ50) were approximately 100 times lower (3-5×10^5 PFU/mL) than that of the parent. Compared with that of YF17D, the emergence of the cytopathic effect (CPE) of the mutant viruses in mammalian cells was delayed. YF17D produced clear plaques on Vero cells after 7 days of infection, Δ10 and Δ77 produced ambiguous plaques at 7 days post-infection (d.p.i.), and no plaques were observed for the Δ20-, Δ30-or Δ50-infected cells until 10 d.p.i. Then immunostaining focus assay was performed to determine the foci of those mutants. The morphology of infectious foci caused by the mutant viruses or YF17D in Vero cells at 6 d.p.i. is shown in Figure 1C. A similar phenomenon was observed in BHK-21 cells (data not shown). The differences in the cytopathogenicity between YF17D and mutant viruses were quantified by measuring the lactate dehydrogenase (LDH) release by Vero cells infected with the same amount (0.05 MOI) of YF17D and mutant viruses. The cell damage caused by the Δ10 and Δ77 mutant strains was comparable but significantly less than that caused by YF17D, and the damage caused by the Δ20, Δ30 and Δ50 mutant strains was comparable but significantly less than that caused by the Δ10 and Δ77 mutant strains (Figure 2A).

To further explore the effects of deletions on viral replication, those deletions were introduced into the YF17D-Nluc replicon (Figure 2B). Luciferase signals at 2 h post-transfection (h.p.t.) showed that none of the deletions affected viral RNA translation which consistent with previous report on WNV[47] and ZIKV.[45] The Δ10 and Δ77 RNA was synthesized as efficiently as that of YF17D (indicated by the luciferase signals at 12–24 h.p.t.) but reached a higher replication plateau; Δ20, Δ30 and Δ50 exhibited significantly slower synthesis efficiency with lower peak signals (Figure 2C). To investigate whether these deletions have a similar effect throughout the entire viral life cycle, one-step growth curve analysis was performed in Vero and C6/36 cells. Compared with YF17D, all the mutant viruses replicated less efficiently, with lower peak titers in Vero cells (Figure 2D). The peak titers of Δ10 (4.7 × 10^6 PFU/mL) and Δ77 (3 × 10^6 PFU/mL) were slightly lower than those of YF17D (1 × 10^7 PFU/mL), while the peak titers of Δ20, Δ30 and Δ50 (3.7–6×10^5 PFU/mL) were more than 10-fold lower than those of YF17D (Figure 2D). The similar results were observed in C6/36 cells (Figure 2E). Given the observed correlation between the flavivirus 3′ UTR and innate immune responses leading to virus attenuation,[32,45,46] we take the advantages of the reporter virus (YF17D-mScarlet) to evaluate the sensitivities. All the mutants were introduced into YF17D-mScarlet backbone. Subsequently, the sensitivity of mutant viruses (17D-muts-mScarlet) and the prototype strain (YF17D-mScarlet) to interferon was examined. The results showed that all the mutant viruses were more sensitive to inhibition by both interferon-β and interferon-γ compared to the prototype strain (Figures 2F and 2G). The sensitivities of viruses to interferon-β and interferon-γ were consistent, decreasing in the following order: Δ50, Δ20, Δ30, Δ10, Δ77, and 17D (Figures 2F and 2G), which was inversely related to viral replication efficiency (Figures 2D and 2E) and viral cytopathogenicity (Figure 2A). In conclusion, deletions in the DB region within the YF17D 3′ UTR increased the vulnerability of YF17D to both type-I and type-II interferons, resulting in attenuated replication and cytopathogenicity.

Mutant viruses are attenuated and immunogenic in mice

The next-generation live attenuated YF vaccine should have a stronger safety profile with at least comparable immunogenicity to that of original YF17D.[48] Next, we evaluated the safety and immunogenicity of the mutant viruses in mouse models. The A129 mice (deficient in IFN-α/β receptors), which are not lethal to YF17D infection but fatal to YFV-Asibi infection,[49] were used to assess the safety and humoral immunogenicity[50,51] of the mutant viruses. Three-to four-week-old A129 mice were immunized with 10^4 PFU of YF17D or mutant virus via the subcutaneous (s.c.) route (Figure 3A). Hyperviremia was detected in YF17D-immunized mice, with peak viremia at day 2 post-immunization and decreasing below the limit of detection (L.O.D) at day 5 (Figure 3B). Regarding the mutant viruses, only Δ10 immunization resulted in much lower viremia in individual mice, and no infectious viruses were detected in other immune sera (Figure 3B). To determine whether the deletions in the 3′ UTR could alter the tissue tropism of YF17D. Multiple mouse organs, including the draining lymph nodes, liver, spleen, bone marrow, and brain, were harvested to test for infectious viruses on day 2, 4, and 6 post-immunization. The YF17D-infected mice exhibited viral loads in all selected organs with peak titers appeared in the following order: the lymph nodes, liver, spleen, bone marrow, and brain (Figure 3C), which reflected the virus dissemination dynamics *in vivo*. In contrast, no viruses were detected in any selected organs of the Δ20-, Δ30-or Δ50-infected mice or in the brains of the Δ10-or Δ77-infected mice (Figure 3C). The Δ10 and Δ77 transiently invaded other organs of A129 mice, and no infectious viruses were detected in all selected organs on day 6 post-immunization (Figure 3C). These results indicate that deletions in the DB region of YF17D result in reduced viscerotropism and loss of neurotropism.

To further confirm the attenuation profile of the mutant viruses, we compared the pathogenicity of the mutant viruses and YF17D in AG129 mice, which are deficient in both IFN-α/β and IFN-γ receptors and highly vulnerable to YF17D infection.[52] Six-to eight-week-old AG129 mice were infected intraperitoneally (i.p.) with a lethal dose (10^4 PFU) of YF17D[52] or the same dose of mutant virus (Figure S1A). The data showed that all mutant viruses were less pathogenic, with lower viremia levels (Figure S1B), higher survival rates (Figure S1C) and less weight loss compared to YF17D (Figure S1D). All Δ20-, Δ30-and Δ50-infected mice survived (Figure S1C), without detectable viremia (Figure S1B). The Δ10-and Δ77-infected mice developed much lower viremia levels (Figure S1B), with survival rates of 44.4% and 77.8%, respectively. While all YF17D-infected mice succumbed to hyperviremia with significant weight loss (Figures S1B–S1D). To investigate whether the difference in pathogenicity was related to viral tissue tropism, mouse organs were collected to detect infectious viruses. The result was basically

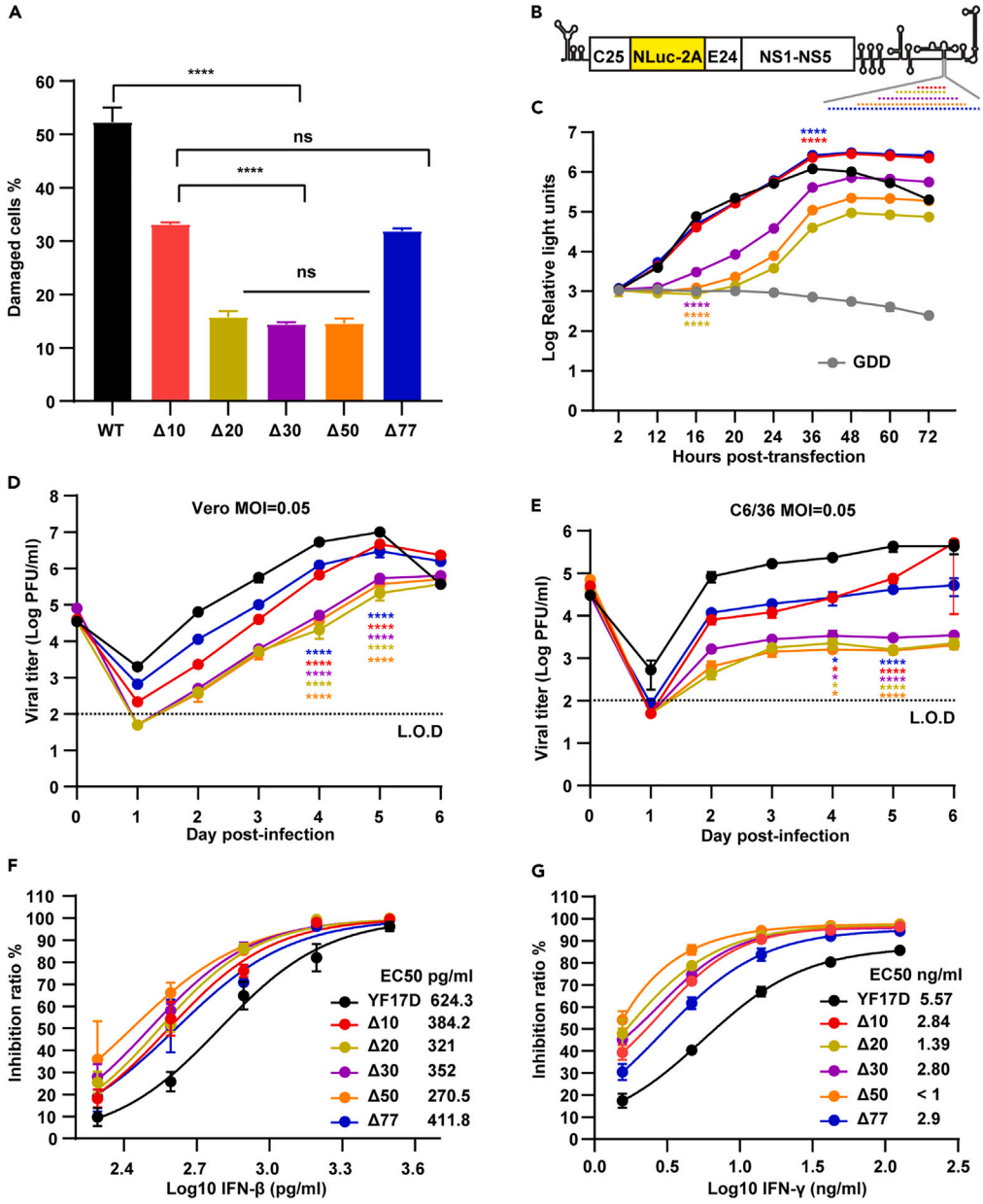

Figure 2. Mutant viruses were attenuated *in vitro*

(A) Mutant viruses caused less cell death than YF17D. Vero cells were infected with YF17D or mutant viruses at an MOI of 0.05, and LDH release in culture medium was quantified on day 8 post-infection to calculate the percentage of damaged cells as described in the STAR Methods.

(B) Schematic diagram of the YF17D replicon. The sequences of YF17D structural gene were replaced with C25-Nluc-2A-E24 to obtain the replicon as described in the STAR Methods section. The dotted lines with different lengths and colors represent the introduction of the Δ10 (red), Δ20 (yellow-green), Δ30 (purple), Δ50 (orange) and Δ77 (blue) mutations into the 3′ UTR.

(C) The effect of the deletions on the replicon assay results. BHK-21 cells were transfected with 10 μg of replicon RNA, and luciferase signals were measured at the indicated time points. Construction with inactivating mutation in GDD (corresponding to residues Gly666, Asp667 and Asp668 in NS5), the conserved functional motif of YF17D RNA polymerase, were used as replicon negative control. Growth curves of YF17D and mutant viruses in Vero cells (D) and in C6/36 cells (E). P0 viruses infected Vero cells at an MOI of 0.05 in 24-well plates, and culture media were harvested daily for live virus detection via plaque assay. EC50 of IFN-β (F) and IFN-γ (G) against YF17D or mutant viruses. Reporter viruses described in the STAR Methods section were used to infect Vero cells at an MOI of 0.1 in black 96-well plates. Cells were treated simultaneously with different concentrations of IFN-β (3125, 1563, 781, 391, or 195 pg/mL) or IFN-γ (126, 42, 14, 4.7 or 1.6 ng/mL). The EC50 value was calculated from the red fluorescent signal after 48 h of incubation. PFU: plaque-forming units. L.O.D.: limit of detection. The data from three independent experiments (A, C, D, and E) are presented as mean ± SD. One-way ANOVA was performed for (A), and two-way ANOVA was used for (C), (D) and (E). *$p < 0.05$, ****$p < 0.0001$, ns = not significant.

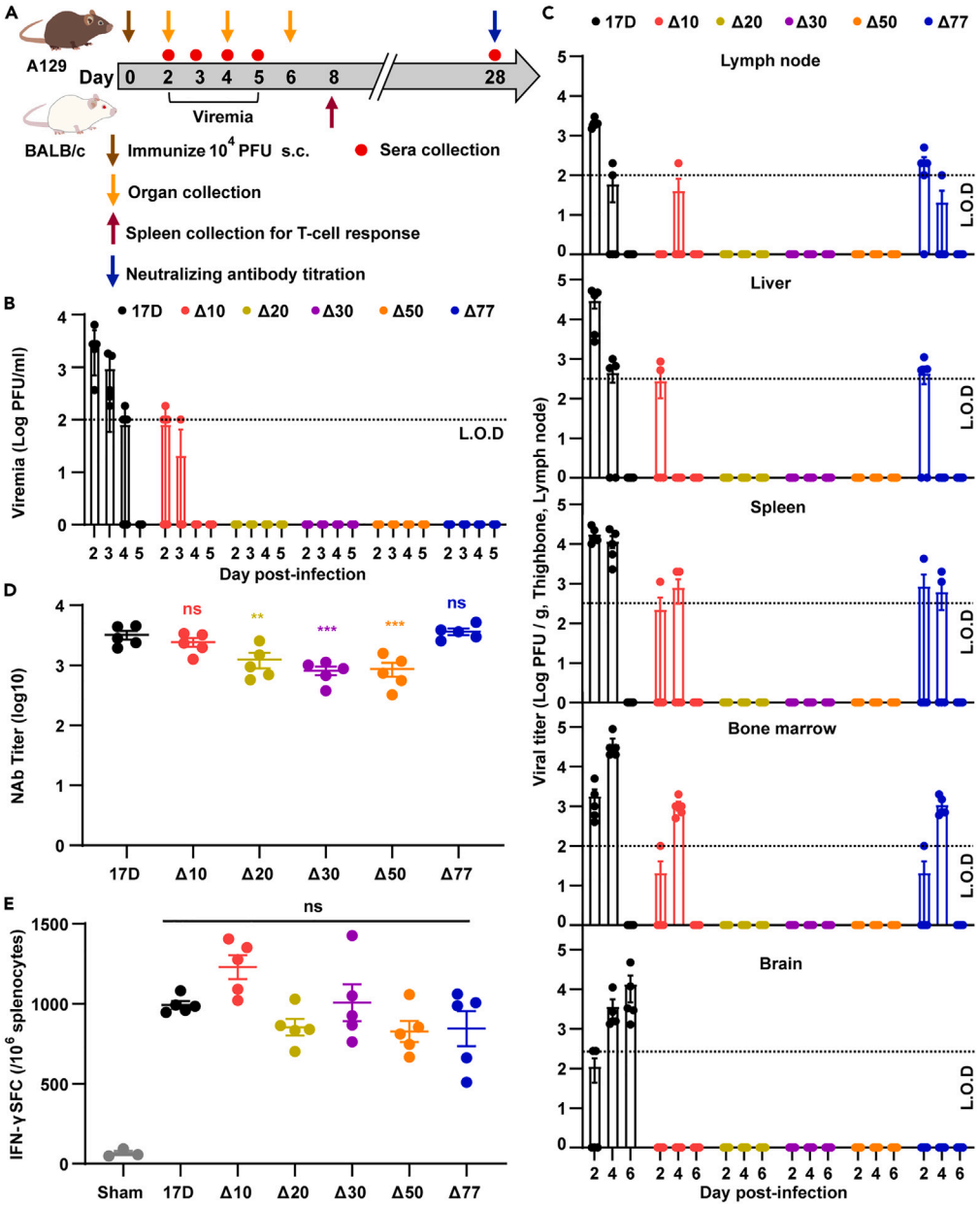

Figure 3. Mutant viruses were attenuated but immunogenic in A129 mice

(A) Experimental procedure schematic. Three-to four-week-old IFNαβR$^{-/-}$ A129 mice and 6- to 8-week-old female BALB/c (H2^{d}) mice (n = 5 per group) were immunized with 10^4 PFU of YF17D or mutant viruses via the s.c. route. The sampling time points and collection metrics are represented by different icons.

(B) Viremia. Viral loads in mouse sera (n = 5 per group) from 2 to 5 days post-infection were measured by plaque assay.

(C) Viral tissue tropism. Five mice in one group were euthanized at 2-, 4-, and 6-day post-infection, and the draining lymph nodes, liver, spleen, bone marrow, and brain were harvested for viral titration after weighing, homogenization and clarification.

(D) Neutralizing antibodies (nAbs) in mouse immune serum. On day 28 post-immunization, nAbs in mouse sera (n = 5) were measured by a 50% reporter signal reduction neutralization test (RRNT50) with YF17D-mScarlet.

(E) Cellular immunity levels determined by ELISpot. On day 8 post-immunization, the splenocytes of viruses or placebo immunized BALB/c (H2^{d}) mice were isolated and stimulated with three YFV E peptides, namely, E60-68 (CYNAVLTHV), E330-338 (CRIPVIVAD) and E133-147 (TKIQYVIRAQLHVGA), *in vitro*. The Y axis indicates the number of cells that specifically secreted IFN-γ. SFC: spot-forming cells. The data are presented as mean ± SEMs. One-way ANOVA was used for (D) and (E). $^{**}p < 0.01$, $^{***}p < 0.001$, ns = not significant.

consistent with that in A129 mice (Figures 3C and S1E). YF17D was disseminated in AG129 mice along the same route (from the lymph node to the liver, spleen, bone marrow, and finally brain) as in A129 mice (Figures 3C and S1E). No infectious particles were detected in the liver, spleen and bone marrow of A129 mice on day 6 post-infection (Figure 3C) while it was detectable in those of AG129 mice (Figure S1E), this may partially explain why YF17D is lethal in the AG129 mouse model but not in the A129 mouse model.[49,52] Regarding the mutant viruses, no infectious viruses were detected in any Δ20-, Δ30-or Δ50-infected mouse organs or in Δ10-infected mouse lymph nodes or brains or in Δ77-infected mouse livers or brains, and less virus was detected in other organs of Δ10-and Δ77-infected mice than that in YF17D-infected mice organs (Figure S1E). Taken together, these findings indicate that the mutant viruses attenuate their pathogenicity in mice by decreasing viscerotropism and abrogating neurotropism. YF17D accumulation in the mouse brain may be the reason for the high probability of YEL-AND.[53]

On day 28 post-immunization, neutralizing antibodies (nAbs) in A129 immune sera were quantified by a reporter virus (YF17D-mScarlet) assay, a similar method was previously used for ZIKV.[45] The results showed that the nAbs induced by Δ10 and Δ77 were comparable to those induced by YF17D, while significantly decreased nAb levels were observed in the Δ20-, Δ30-and Δ50-immunized mouse sera (Figure 3D); this difference may be due to the inability of these strains to replicate effectively *in vivo* (Figures 3C and S1E).

We also evaluated the cellular immune responses induced by these mutant viruses in a BALB/c mouse model.[54] At day 8 post s.c. injection of 10^4 PFU of YF17D or mutant viruses or placebo, the splenocytes of the BALB/c mice were isolated and stimulated with three YFV E peptides[54] to enumerate IFN-γ-secreting cells via an ELISpot assay. The results showed that compared with sham group all the mutant viruses triggered the activation of YFV-specific T cells in BALB/c mice at levels comparable to those induced by YF17D (Figure 3E). In other words, the cellular immunity induced by the mutant viruses is comparable to that induced by YF17D. Weighing the balance of safety and immunity of a quality vaccine, the Δ10 was excluded because of its higher lethality in AG129 mice (Figure S1C), and Δ20, Δ30 and Δ50 were excluded because of their induction of lower nAb levels (Figure 3D). Therefore, the Δ77 was selected as the optimal vaccine candidate for subsequent studies.

YF17D-Δ77 protects A129 mice from lethal challenge with YFV-Asibi

To assess the efficacy of YF17D-Δ77, A129 mice which immunized by YF17D-Δ77 were challenged with 10^6 PFU of YFV-Asibi via the i.p. route on day 28 post-immunization (Figure 4A). Due to dose-sparing strategies have been used to address vaccine shortages,[23] we established high- (10^4 PFU) and low-dose (10 PFU) immunization groups to determine the minimum dose requirement for protection (Figure 4A). The nAb titers on day 28 post-immunization were measured by two methods: a 50% reporter signal reduction neutralization test (RRNT50) with YF17D-mScarlet (Figure 4B) and a 50% plaque reduction neutralization test (PRNT50) with YFV-Asibi (Figure 4C). Although the PRNT50 value was much lower than the RRNT50 value, both results led us to reach the same conclusions: (i) YF17D-Δ77 elicited the production of nAbs at levels comparable to that elicited by YF17D in both the high- and low-dose groups; and (ii) even with a 10 PFU dose, YF17D-Δ77 still induced the production of similar nAb levels (Figures 4B and 4C).

All immunized mice were completely protected from lethal challenge against YFV-Asibi and survived without detectable viremia (Figures 4D and 4F), viral RNA loads in organs (brain, liver, spleen and bone marrow) (Figure 4E) and weight loss (Figure 4G). In contrast, all the placebo-treated mice developed severe disease symptoms, such as piloerection, hunched back, sluggishness, or orbital tightening.[51] On day 2 post-challenge, hyperviremia was observed (Figure 4D); at 6 days post-challenge, high levels of viral RNA were detected in brain, liver, spleen, and bone marrow (Figure 4E); and at 6–8 days after challenge, all the mice lost more than 20% of initial body weight and were euthanized (Figures 4F and 4G). In conclusion, both high (10^4 PFU) and low (10 PFU) doses of YF17D-Δ77 administered in a single shot provided protection to mice against lethal YFV-Asibi challenge.

Single dose of YF17D-Δ77 provides durable immune protection in mice

YF17D induces durable humoral and cellular immune responses in humans, conferring life-long immune protection with a single dose.[16] Next, we examined the long-term immune potency of YF17D-Δ77 (Figure 5A). A129 mice were immunized with 10^4 PFU of YF17D or YF17D-Δ77 or mock-immunized with 100 μL of PBS. The nAbs were measured at 8-, 16-, 32- and 50-week post-immunization (Figure 5A). The data showed that the nAbs in the sera of mice immunized with YF17D-Δ77 were maintained at high levels throughout the entire monitoring period and were comparable to those in YF17D-immunized mice (Figure 5B). Two days after the last blood collection, the A129 mice were challenged with YFV-Asibi, and all immunized mice survived from the challenge without detectable viremia (Figure 5D), visible illness, and any body weight loss (Figure 5F), while 3/5 of the mock-immunized mice reached the end of their life within 9 days (Figure 5E), and the other 2/5 mice recovered from obvious disease symptoms but experienced significant weight loss (Figures 5E and 5F). Since YF17D-induced humoral and cellular immunity work together to provide long-lasting immune protection in humans,[55] we tested the persistence of cellular immunity in YF17D-Δ77-immunized BALB/c mice. Six months after immunization, IFN-γ-secreting cells were still detected in the spleens of mice at levels comparable to those in YF17D-immunized mice (Figure 5C). In summary, single dose of YF17D-Δ77 can provide long-lasting immune protection in mouse models.

The stability of attenuation and immunogenicity are maintained in YF17D-Δ77 after successive passages in Vero cells

An excellent live attenuated vaccine needs to be stable during production, including sequence, safety and immunogenicity stability.[56] To assess the stability of YF17D-Δ77, we conducted 20 rounds of blind passaging of YF17D-Δ77 in Vero cells, and three independent trials were performed. Whole-genome sequencing confirmed the stable presence of rΔ77 mutation in three virus strains at P20 generation, and four consistent mutations were identified, including a missense mutation (H280R) and a nonsense mutation (T1876C) in the E gene, a nonsense

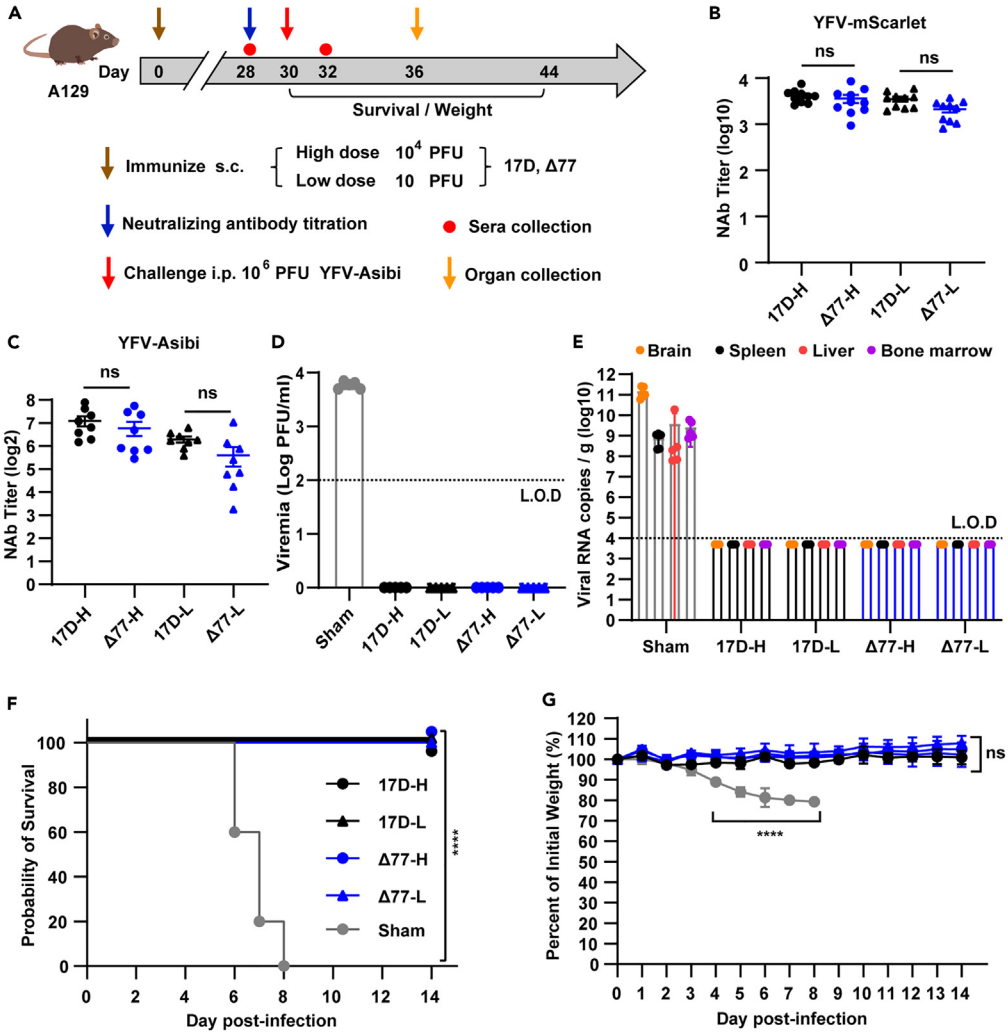

Figure 4. YF17D-Δ77 protected mice against WT YFV challenge

(A) Experimental procedure schematic. Three-to four-week-old IFNαβR$^{-/-}$ A129 mice were subcutaneously immunized with a high dose (10^4 PFU) or low dose (10 PFU) of YF17D-Δ77 or YF17D and intraperitoneally challenged with 10^6 PFU of YFV-Asibi. The sampling time points and collection metrics are represented by different icons. NAbs measured by (B) RRNT50 and (C) PRNT50. Mouse sera (n = 10) were collected on day 28 post-immunization and nAbs were quantified by a 50% reporter signal reduction neutralization test (RRNT50) with YF17D-mScarlet and a 50% plaque reduction neutralization test (PRNT50) with YFV-Asibi. The black circle represents a high dose of YF17D, the black triangle represents a low dose of YF17D, the blue circle represents a high dose of YF17D-Δ77, and the blue triangle represents a low dose of YF17D-Δ77.

(D) Viremia post-challenge. On day 30 post-immunization, the mice (n = 10) were challenged with 10^6 PFU of YFV-Asibi via the i.p. route. On day 2 post-challenge, infectious viruses in the mouse serum (n = 5) were measured via plaque assay.

(E) Viral RNA copies in mouse organs after challenge. On day 6 post-challenge, the mice (n = 5) were euthanized, and the brains, spleens, livers and bone marrow were harvested and subjected to weighing, homogenization and clarification before viral titration via plaque assay. Survival (F) and weight change (G) of the mice post-challenge. The mice (n = 5) underwent 14 days of health monitoring after challenge and were euthanized when their body weight lost by 20%. The data in (B) and (C) are presented as mean ± SEMs; the data in (D), (E) and (G) are presented as mean ± SD. One-way ANOVA was used for (B) and (C); log rank tests were performed for (H); multiple t tests were used for (G). ****$p < 0.0001$, ns = not significant.

mutation (A6910G) in the NS4A gene and a missense mutation (N391K) in the NS5 gene, which accumulated in all three P20 strains (Table 1). Furthermore, an additional ongoing substitution (A146V) was identified in the NS4A gene of P20-2 strain, while another substitution (G196V) was found in the NS1 gene of P20-3 strain (marked in blue font in Table 1). The three P20 strains produced heterogeneous plaques in BHK-21 cells (Figure 6A), indicating that each viral stock was a mixture of multiple viruses. However, the average plaque size of the P20 viruses was comparable to that of the P0 virus (Figure 6A). Next, we compared the replication kinetics of the P20 viruses with those of the P0 virus, and the data showed that P20 viruses exhibited significantly enhanced replication efficiency compared to the P0 virus in Vero cells (Figure 6B), which suggested that the mutations listed in Table 1 resulted from virus adaptation to growth in Vero cells.

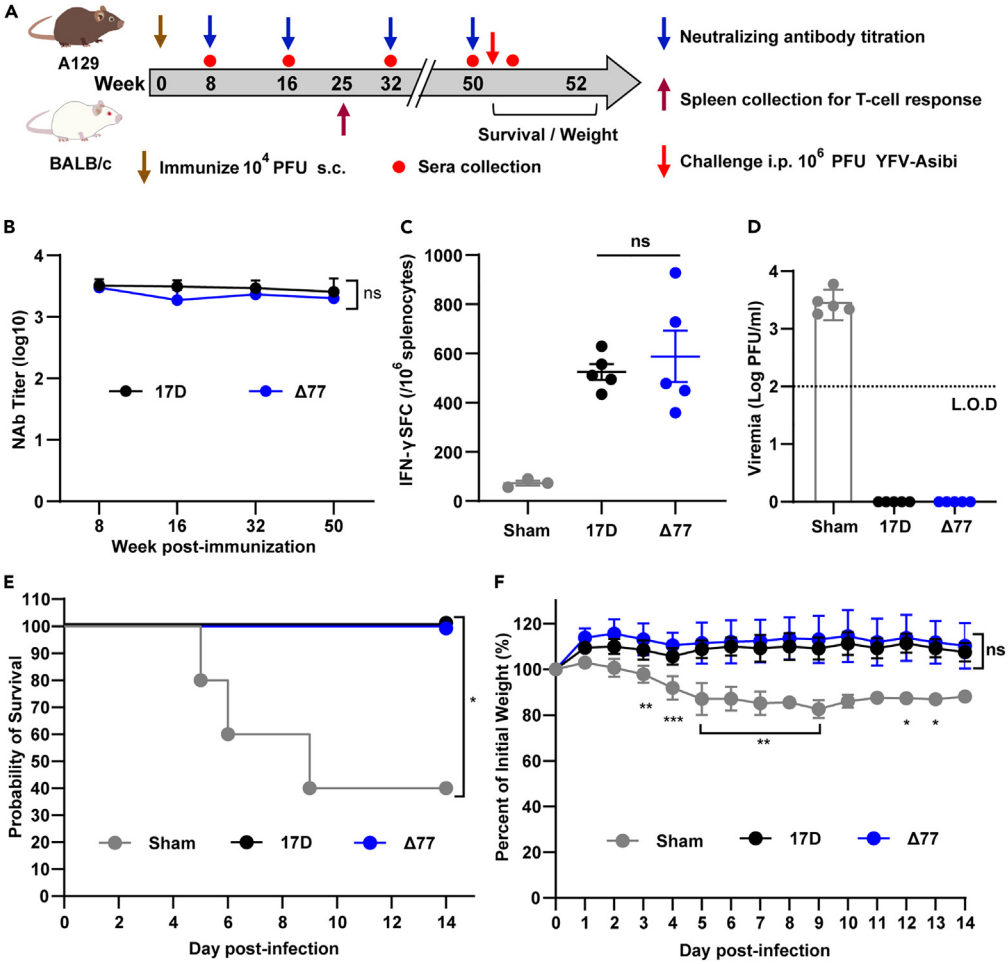

Figure 5. Single dose of YF17D-Δ77 provides durable immune protection in mice

(A) Experimental procedure schematic. Three-to four-week-old IFNαβR$^{-/-}$ A129 mice and 6- to 8-week-old female BALB/c (H2^{d}) mice (n = 5 per group) were immunized with 10^4 PFU of YF17D or YF17D-Δ77 via the s.c. route. The sampling time points and collection metrics are represented by different icons.

(B) NAbs in immune sera. Mouse sera at 8-, 16-, 32-, and 50-week post-immunization were collected to quantify the nAbs by RRNT50.

(C) Cellular immunity. Splenocytes were isolated from BALB/c (H2^{d}) mice at 50 weeks after immunization, and IFN-γ-secreting cells were assessed by ELISpot.

(D) Viremia post-challenge. Two days after the last blood collection, the mice were challenged with 10^6 PFU of YFV-Asibi, and on day 2 post-challenge, mouse sera were collected to detect infectious viruses by plaque assay. Survival (E) and weight change (F) of mice post-challenge. The mice were subjected to 14 days of health monitoring after the challenge and were euthanized when their body weight decreased by 20%. The data in (B) and (C) are presented as mean ± SEMs; the data in (D) and (F) are presented as mean ± SD. two-way ANOVA and one-way ANOVA were used for (B) and (C), respectively; log rank tests were performed for (E); multiple t tests were used for (F). *$p < 0.05$, **$p < 0.01$, ***$p < 0.001$, ns = not significant.

To confirm the safety of the P20 viruses, P20-2 and P20-3, which had more cell-adaptive mutations, were i.p. injected into AG129 mice. During the 30-day observation, the mice showed no signs of illness and all survived (Figure 6C) without any weight loss (data not shown). Next, we immunized A129 mice with P20-2, and 100% seroconversion with high levels of nAbs was observed (Figure 6D), which fully protected the mice from challenge with YFV-Asibi (Figures 6E–6H). Despite lower levels of nAbs observed in sera from mice immunized with a lower dose (Figure 6D), complete protections were still conferred (Figures 6E–6H). In conclusion, after consecutive passaging of YF17D-Δ77 in Vero cells, the Δ77 mutation stably persisted for at least 20 passages, and the P20 viruses maintain attenuated and immunogenic properties despite the emergence of cell-adaptive mutations.

DISCUSSION

Although there is an approved highly effective live attenuate vaccine (YF17D) for the prevention of YF, frequent resurgences of YF have placed 900 million people in 47 countries in Africa and the Americas at significant risk of YFV infection.[21,57] The special manufacturing processes (in specific pathogen-free chicken embryos) limit vaccine production,[3] leading to an insufficient supply of vaccine during large outbreaks.[1,8,15] In addition, due to inherent risks associated with YF17D and production process,[17,58] a significant number of groups, including infants under

Table 1. Mutations in passaged YF17D-Δ77

	E	NS1	NS4A	NS5	3′UTR
P20-1[a]	H280R(A1812G)[b] (T1876C)		(A6910G)	N391K (C8809A)	Δ77
P20-2	H280R (A1812G) (T1876C)		(A6910G) A146V(C6876T)[c]	N391K (C8809A)	Δ77
P20-3	H280R (A1812G) (T1876C)	G196V(G3039T)[c]	(A6910G)	N391K (C8809A)	Δ77

[a]Whole-genome sequencing was performed for three P20 viral strains of YF17D-Δ77.
[b]The content before the parentheses indicates the change in amino acid, and the content inside the parentheses indicates the change in nucleotide.
[c]Mutations that appear as overlapping peaks in the Sanger sequencing results.

9 months of age, pregnant and lactating women, elderly individuals over 60 years old, individuals in a severe immunocompromised state, and egg-hypersensitive individuals, are either restricted from or excluded from vaccination.[19] In YF high-risk regions, these groups collectively represent a considerable proportion of the population, however, there is no well-established prevention strategy for them.[48]

Driven by the Eliminate Yellow Fever Epidemics (EYE) Strategy, more than 10 new YF vaccine candidates are in different stages of development to enhance the global vaccine stockpile, enable better respond to emergencies.[48] The inactivated candidate XRX-001[59] and the recombinant viral vector candidate MVA-BN-YF[60] have been tested in phase I clinical trials. Despite the sufficient safety of XRX-001, two doses of XRX-001 were required for vaccination to induce the sufficient protective nAbs in macaques, resulting in poor immune durability.[59] Similarly, MVA-BN-YF also requires multiple doses to confer protection comparable to that of a single dose of YF17D.[48] Therefore, neither is an optimal candidate for outbreak scenarios nor mass vaccination campaigns, and no phase II trial has been scheduled for them.[48] The most recently developed mRNA vaccine candidates also require two injections to induce the production of slightly lower levels of nAb in rhesus macaques than does a single injection of YF17D, but passively transferred immune sera were able to provide complete protection in mice.[51] The 17D-IRES (obtained from an infectious clone of YF17D) showed a better safety profile, but only two-step immunization results are available,[61] and sufficient data to support 17D-IRES as a superior vaccine candidate are lacking. For other novel vaccine candidates, there is a lack of sufficient evidence and further exploration to prove their promise.[48] Therefore, the development of effective and safer next-generation YF vaccines remains highly needed.

Flavivirus 3′ UTRs have attracted significant attention for live attenuated vaccine design.[35] The 3′ UTR of YF17D contains only 4 bases that different from the parental YFV-Asibi, and its structure conforms to the basic characteristics of the flavivirus 3′ UTR.[53] However, since YF17D has been developed as an effective live attenuated vaccine for almost a century and its attenuation mechanism remains undetermined,[53] the relationship between the 3′ UTR and YFV virulence is often overlooked.

Here, we report a safer live attenuated YF vaccine candidate, YF17D-Δ77, which is further attenuated by removal of the DB domain in the YF17D 3′ UTR and maintains comparable immunogenicity to YF17D. Initially, we designed a series of overlap deletions (Δ10, Δ20, Δ30, Δ50, and Δ77) in the DB region of the YF17D 3′ UTR, similar to what we previously reported for ZIKV.[45] We found that these deletions reduced the cytopathogenicity of YF17D, and the attenuation was independent from the length of the deletion. The phenotype of the Δ10 and Δ77 mutations on viral cytopathogenicity were comparable but less than those of the Δ20, Δ30 and Δ50 mutations, and the latter three mutations had similar effects on viral cytopathogenicity. Meanwhile, these deletions also attenuated the pathogenicity of YF17D in AG129 mice, but the Δ10 mutant caused higher mortality than did the Δ77 mutant. The attenuation mechanism of the 3′ UTR mutant viruses seem to be related to reduced replication efficiency due to the increased sensitivity of the viruses to type I and type II interferon responses. The inhibition by the interferon response does not appear to play a critical role in RNA synthesis because the viral RNA synthesis efficiency of Δ10 and Δ77 was not lower than that of YF17D, while the replication efficiency was significantly reduced.

One of the direct causes of the attenuation of mutant viruses *in vivo* is a shift in viral tissue tropism. YF17D spreads sequentially through the draining lymph nodes, liver, spleen, bone marrow, and brain in mice and accumulates in the mouse brain, which may explain why adverse events caused by YF17D are usually neurotropic diseases.[58] YF17D had similar tissue tropisms in A129 mice and AG129 mice, but no live virus was detected in the liver, spleen, or bone marrow of A129 mice while it was detected in AG129 mice at 6 d.p.i., which may explain why YF17D was not lethal to A129 mice but lethal to AG129 mice.[49,52] However, only the Δ10 and Δ77 mutants caused transient infection of organs other than the brain of A129 mice and the brain and liver of AG129 mice. That is, all 3′ UTR mutant viruses lost their neurotropism and exhibited reduced viscerotropism.

Moreover, it is encouraging that all 3′ UTR mutant viruses were highly immunogenic. Since the low replication efficiency of YF17D-Δ20, YF17D-Δ30 and YF17D-Δ50 led to weaker humoral immunity and YF17D-Δ10 exhibited greater lethality in AG129 mice, we ultimately selected YF17D-Δ77 as the optimal live attenuated vaccine candidate. As a live attenuated vaccine candidate, YF17D-Δ77 has all the excellent properties of its parent: (i) a single injection can elicit robust humoral and cellular immune responses and provide complete protection in mice; and (ii) a single immunization provides long-lasting protection. In the long-term immune effect study, the reduced lethality of YFV-Asibi in aged A129 mice (Figures 5E and 5F) may be related to age-dependent resistance,[62] the two survival mice in the sham group developed obvious signs of disease, while all the mice in the immune group survived in good health (Figures 5E and 5F). As vaccines are often in short supply,[21] we explored the minimum requirement dose and found that even with a 10 PFU dose, YF17D and YF17D-Δ77 still conferred completely

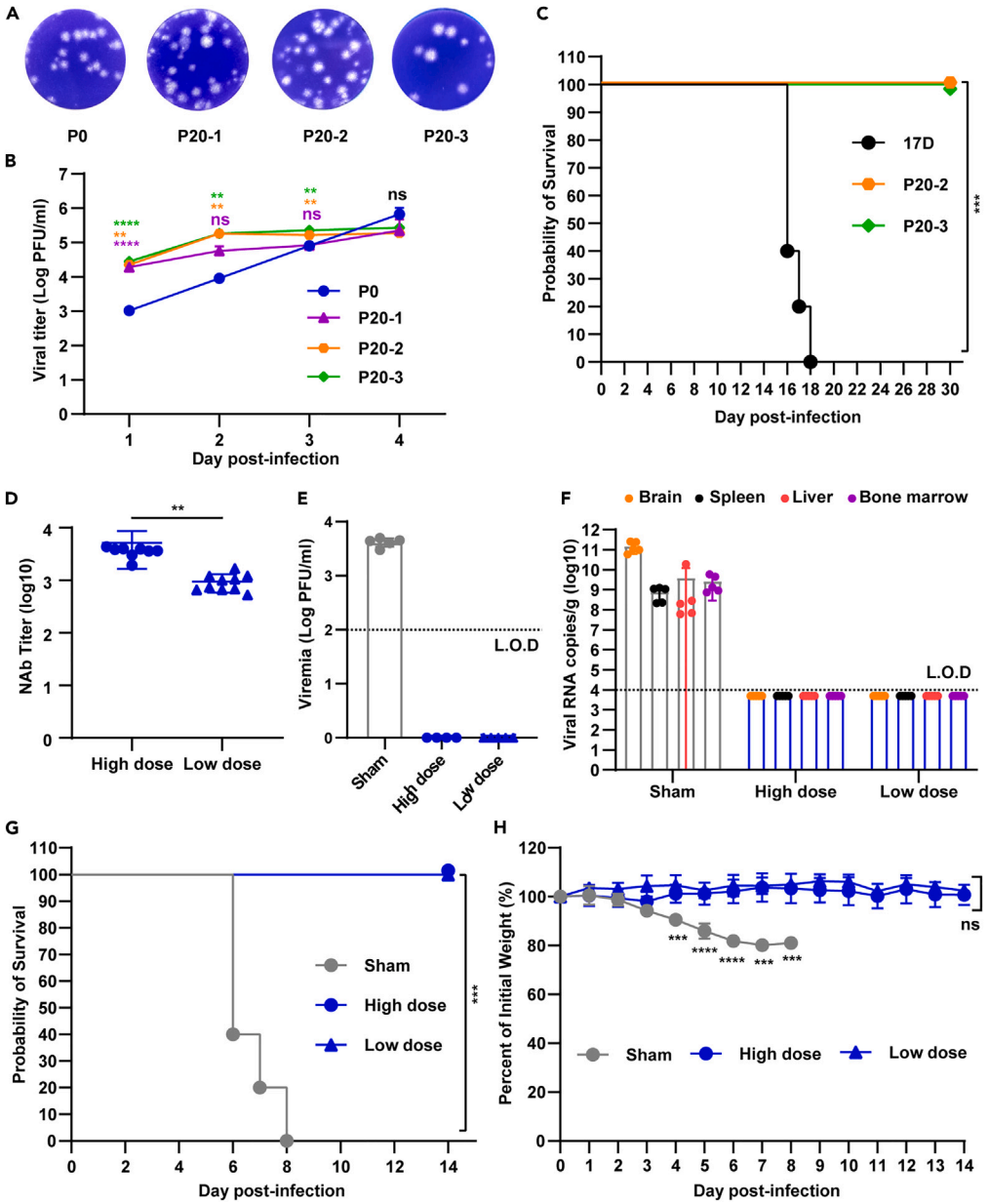

Figure 6. The stability of attenuation and immunogenicity are maintained in YF17D-Δ77 after successive passages in Vero cells

(A) Plaque morphology of passaged YF17D-Δ77. Three P20 YF17D-Δ77 strains were obtained in 3 independent trials of 20 rounds of blind passaging of P0 YF17D-Δ77 in Vero cells and were titrated by plaque assay.

(B) Replication curves of P20 YF17D-Δ77 strains. Vero cells in 24-well plates were infected with P0, P20-1, P20-2 or P20-3 YF17D-Δ77 at an MOI of 0.05, and the amplified viruses in the culture medium were quantified daily by plaque assay.

(C) Survival of the AG129 mice. Six-to eight-week-old AG129 mice (n = 5) were i.p. injected with 10^4 PFU of P0, P20-2 or P20-3 YF17D-Δ77, and the health status was accessed daily for 30 days. The mice were euthanized when their body weight decreased by 20%.

(D–H) Immunoprotective efficacy of P20 YF17D-Δ77 in mice. Three-to four-week-old IFNαβR$^{-/-}$ A129 mice (n = 10) were immunized with a high or low dose of P20-2 YF17D-Δ77, and on day 28 post-immunization, the serum nAb concentration in the mice was measured by RRNT50 (D). On day 30 post-immunization, the mice were challenged with YFV-Asibi, and on day 2 post-challenge, viremia was tested by plaque assay (E). On day 6 post-challenge, viral RNA copies were detected in mouse organs (brain, spleen, liver and bone marrow) (F). Survival curve (G) and body weight change curve (H) of the mice (n = 5) were plotted based on the monitoring results during the 14 days post-challenge. The data in panels (B, D, E, F, and H) are presented as mean ± SD. Multiple t tests and t tests were performed for (B and H) and (D), respectively; log rank tests were used for (C and G). $^{**}p < 0.01$, $^{***}p < 0.001$, $^{****}p < 0.0001$, ns = not significant.

protection in mice. With respect to the possibility of recovering the artificial deletion (Δ77) in YF17D-Δ77, we verified the genetic stability of YF17D-Δ77 in Vero cells and found that the Δ77 mutation as stably present for at least 20 generations. Although several cell-adaptive mutations appeared in P20 viruses, we preliminarily identified that these adaptive mutations did not affect viral pathogenicity or immunogenicity.

Pregnant and lactating women are restricted from receiving YF17D to avoid the risk of mother-to-child transmission, as YF17D is neurotropic, and the risk to infants is higher.[20,58] Nevertheless, the WHO notes that the benefits may outweigh the disadvantages of vaccinating these groups during severe outbreaks.[48] Non-neurotropic YF17D-Δ77 could compensate for this risk. Although there are huge physiological differences between mice and humans, YFV-infected mice can still partially mimic human infection, such as causing viremia and tropism of tissues such as the brain, spleen, and liver (Figures 3D and 3E). Severe human infections often end in death from multi-organ failure mainly in the liver, while the brain exhibited the highest viral load in the lethal infections of mice, the load of virus in brain tissue is the highest, and the pathological changes of brain, liver, and spleen were not enough to explain the cause of death in mice (data not shown). The WHO has designated the NHPs, which are more closely related to humans, as the only animal model for YFV vaccine development and evaluation, but due to its high cost and unreadily available experimental conditions, many preclinical preliminary studies still use mouse models as the preferred options,[50,51,63,64] and some research groups showed that the good immune response of vaccine in mice can be reproduced in human[59,63] or NHPs.[51] In summary, our results support the further development of YF17D-Δ77 in NHPs to accelerate its clinical application. Moreover, new vaccine manufacturing technologies need to be developed to increase vaccine production. Since YF17D-Δ77 is derived from an infectious clone, it will likely be produced in Vero cells, as *Fabienne* described,[50] to achieve high yields. Mechanistically, further studies are needed to explore why the absence of a large fragment (Δ77) did not result in more attenuation. In conclusion, we developed a safer live attenuated YF vaccine that may address the shortcomings of YF17D.

Limitations of the study

In this study, we developed a new live attenuated yellow fever vaccine, YF17D-Δ77, which is safer than YF17D and exhibits equivalent immunogenicity and efficacy. However, we just evaluated it in mouse models. Further research is needed in the NHP animal model to accelerate its clinical application. In addition, we have observed differences in the impact of various deletions in the 3′ UTR of YF17D genome on viral virulence, but we have not delved into the reasons. Therefore, further studies are needed to explore this. There are structural commonalities in the 3′ UTR of flaviviruses; whether the reduced virulence caused by deletion mutations in this study can be extended to other members of the *Flaviviridae* family also needs to be verified.

RESOURCE AVAILABILITY

Lead contact

Further information and requests for resources should be directed to and will be fulfilled by the lead contact, Shan Chao (shanchao@wh.iov.cn).

Materials availability

The plasmids generated in this study are maintained at Wuhan Institute of Virology, Chinese Academy of Sciences and may be available upon request from the lead contact, Shan Chao (shanchao@wh.iov.cn).

Data and code availability

- The datasets generated and analyzed related to this paper are available from the lead contact on reasonable request.
- This paper does not report original code.
- Any additional information required to reanalyze the data reported in this paper is available from the lead contact upon request.

ACKNOWLEDGMENTS

We thank the Public Technology Service Center of the Wuhan Institute of Virology for providing technical assistance. This study was financially supported by the STS regional key project (KFJ-STS-QYZD-2021-12-001 S.C.) from Chinese Academy of Sciences. We are grateful to the Center for Animal Experiments staff and National Biosafety Laboratory Level 3 at the Wuhan Institute of Virology. We thank Dr. Pei-Yong Shi from University of Texas Medical Branch for his guidance and support.

AUTHOR CONTRIBUTIONS

W.G. designed and performed the experiments, organized the data, and wrote the manuscript, T.J., J.R., X.Z., and C.Y. participated in the challenge experiment, J.R., J.S., and Z.Z. participated in the ELISpot experiment, Z.Z. participated in the experiments of mice tissue tropism of mutant strains, J.S., C.Y., and M.L. participated in blood collection, J.S. participated in RRNT50 assay, X.H. contributed to laboratory maintenance, C.S. conceived the study, supervised the experiments, and revised the manuscript.

DECLARATION OF INTERESTS

The authors declare no competing interests.

STAR★METHODS

Detailed methods are provided in the online version of this paper and include the following:

SUPPLEMENTAL INFORMATION

Supplemental information can be found online at https://doi.org/10.1016/j.isci.2024.110972.

Received: May 2, 2024
Revised: July 7, 2024
Accepted: September 13, 2024
Published: September 17, 2024

REFERENCES

1. Pierson, T.C., and Diamond, M.S. (2020). The continued threat of emerging flaviviruses. Nat. Microbiol. *5*, 796–812. https://doi.org/10.1038/s41564-020-0714-0.
2. Rice, C.M., Lenches, E.M., Eddy, S.R., Shin, S.J., Sheets, R.L., and Strauss, J.H. (1985). Nucleotide sequence of yellow fever virus: implications for flavivirus gene expression and evolution. Science *229*, 726–733. https://doi.org/10.1126/science.4023707.
3. Monath, T.P., and Vasconcelos, P.F.C. (2015). Yellow fever. J. Clin. Virol. *64*, 160–173. https://doi.org/10.1016/j.jcv.2014.08.030.
4. Ramos-Lorente, S., Romero-López, C., and Berzal-Herranz, A. (2021). Information Encoded by the Flavivirus Genomes beyond the Nucleotide Sequence. Int. J. Mol. Sci. *22*, 3738. https://doi.org/10.3390/ijms22073738.
5. Ndeffo-Mbah, M.L., and Pandey, A. (2020). Global Risk and Elimination of Yellow Fever Epidemics. J. Infect. Dis. *221*, 2026–2034. https://doi.org/10.1093/infdis/jiz375.
6. Gianchecchi, E., Cianchi, V., Torelli, A., and Montomoli, E. (2022). Yellow Fever: Origin, Epidemiology, Preventive Strategies and Future Prospects. Vaccines (Basel) *10*, 372. https://doi.org/10.3390/vaccines10030372.
7. Gaythorpe, K.A., Hamlet, A., Jean, K., Garkauskas Ramos, D., Cibrelus, L., Garske, T., and Ferguson, N. (2021). The global burden of yellow fever. Elife *10*, e64670. https://doi.org/10.7554/eLife.64670.
8. Vasconcelos, P.F.C., and Monath, T.P. (2016). Yellow Fever Remains a Potential Threat to Public Health. Vector Borne Zoonotic Dis. *16*, 566–567. https://doi.org/10.1089/vbz.2016.2031.
9. Quaresma, J.A.S., Duarte, M.I.S., and Vasconcelos, P.F.C. (2006). Midzonal lesions in yellow fever: a specific pattern of liver injury caused by direct virus action and *in situ* inflammatory response. Med. Hypotheses *67*, 618–621. https://doi.org/10.1016/j.mehy.2006.01.060.
10. Frierson, J.G. (2010). The yellow fever vaccine: a history. Yale J. Biol. Med. *83*, 77–85.
11. Theiler, M., and Smith, H.H. (1937). The Use of Yellow Fever Virus Modified By In Vitro Cultivation For Human Immunization. J. Exp. Med. *65*, 787–800. https://doi.org/10.1084/jem.65.6.787.
12. Poland, J.D., Calisher, C.H., Monath, T.P., Downs, W.G., and Murphy, K. (1981). Persistence of neutralizing antibody 30-35 years after immunization with 17D yellow fever vaccine. Bull. World Health Organ. *59*, 895–900.
13. Ortiz-Martínez, Y., Patiño-Barbosa, A.M., and Rodriguez-Morales, A.J. (2017). Yellow fever in the Americas: the growing concern about new epidemics. F1000Res. *6*, 398. https://doi.org/10.12688/f1000research.11280.2.
14. Chippaux, J.P., and Chippaux, A. (2018). Yellow fever in Africa and the Americas: a historical and epidemiological perspective. J. Venom. Anim. Toxins Incl. Trop. Dis. *24*, 20. https://doi.org/10.1186/s40409-018-0162-y.
15. Diagne, M.M., Ndione, M.H.D., Gaye, A., Barry, M.A., Diallo, D., Diallo, A., Mwakibete, L.L., Diop, M., Ndiaye, E.H., Ahyong, V., et al. (2021). Yellow Fever Outbreak in Eastern Senegal, 2020-2021. Viruses *13*, 1475. https://doi.org/10.3390/v13081475.
16. Barrett, A.D.T., and Teuwen, D.E. (2009). Yellow fever vaccine - how does it work and why do rare cases of serious adverse events take place? Curr. Opin. Immunol. *21*, 308–313. https://doi.org/10.1016/j.coi.2009.05.018.
17. Seligman, S.J., and Casanova, J.L. (2016). Yellow fever vaccine: worthy friend or stealthy foe? Expert Rev. Vaccines *15*, 681–691. https://doi.org/10.1080/14760584.2016.1180250.
18. Monath, T.P. (2005). Yellow fever vaccine. Expert Rev. Vaccines *4*, 553–574. https://doi.org/10.1586/14760584.4.4.553.
19. Hansen, C.A., and Barrett, A.D.T. (2021). The Present and Future of Yellow Fever Vaccines. Pharmaceuticals *14*, 891. https://doi.org/10.3390/ph14090891.
20. Tomashek, K.M., Challberg, M., Nayak, S.U., and Schiltz, H.F. (2019). Disease Resurgence, Production Capability Issues and Safety Concerns in the Context of an Aging Population: Is There a Need for a New Yellow Fever Vaccine? Vaccines (Basel) *7*, 179. https://doi.org/10.3390/vaccines7040179.
21. (2017). Eliminate Yellow fever Epidemics (EYE): a global strategy, 2017–2026. Wkly. Epidemiol. Rec. *92*, 193–204.
22. Barrett, A.D.T. (2016). Yellow Fever in Angola and Beyond–The Problem of Vaccine Supply and Demand. N. Engl. J. Med. *375*, 301–303. https://doi.org/10.1056/NEJMp1606997.
23. Wu, J.T., Peak, C.M., Leung, G.M., and Lipsitch, M. (2016). Fractional dosing of yellow fever vaccine to extend supply: a modelling study. Lancet *388*, 2904–2911. https://doi.org/10.1016/s0140-6736(16)31838-4.
24. Nathan, N., Barry, M., Van Herp, M., and Zeller, H. (2001). Shortage of vaccines during a yellow fever outbreak in Guinea. Lancet *358*, 2129–2130. https://doi.org/10.1016/s0140-6736(01)07185-9.
25. Wilder-Smith, A., and Leong, W.Y. (2017). Importation of yellow fever into China: assessing travel patterns. J. Travel Med. *24*, tax008. https://doi.org/10.1093/jtm/tax008.
26. Corver, J., Lenches, E., Smith, K., Robison, R.A., Sando, T., Strauss, E.G., and Strauss, J.H. (2003). Fine mapping of a cis-acting sequence element in yellow fever virus RNA that is required for RNA replication and cyclization. J. Virol. *77*, 2265–2270. https://doi.org/10.1128/jvi.77.3.2265-2270.2003.

27. Alvarez, D.E., De Lella Ezcurra, A.L., Fucito, S., and Gamarnik, A.V. (2005). Role of RNA structures present at the 3'UTR of dengue virus on translation, RNA synthesis, and viral replication. Virology *339*, 200–212. https://doi.org/10.1016/j.virol.2005.06.009.
28. Manzano, M., Reichert, E.D., Polo, S., Falgout, B., Kasprzak, W., Shapiro, B.A., and Padmanabhan, R. (2011). Identification of cis-acting elements in the 3'-untranslated region of the dengue virus type 2 RNA that modulate translation and replication. J. Biol. Chem. *286*, 22521–22534. https://doi.org/10.1074/jbc.M111.234302.
29. Mutebi, J.P., Rijnbrand, R.C.A., Wang, H., Ryman, K.D., Wang, E., Fulop, L.D., Titball, R., and Barrett, A.D.T. (2004). Genetic relationships and evolution of genotypes of yellow fever virus and other members of the yellow fever virus group within the Flavivirus genus based on the 3' noncoding region. J. Virol. *78*, 9652–9665. https://doi.org/10.1128/jvi.78.18.9652-9665.2004.
30. Villordo, S.M., Carballeda, J.M., Filomatori, C.V., and Gamarnik, A.V. (2016). RNA Structure Duplications and Flavivirus Host Adaptation. Trends Microbiol. *24*, 270–283. https://doi.org/10.1016/j.tim.2016.01.002.
31. Gritsun, T.S., and Gould, E.A. (2006). Direct repeats in the 3' untranslated regions of mosquito-borne flaviviruses: possible implications for virus transmission. J. Gen. Virol. *87*, 3297–3305. https://doi.org/10.1099/vir.0.82235-0.
32. Manokaran, G., Finol, E., Wang, C., Gunaratne, J., Bahl, J., Ong, E.Z., Tan, H.C., Sessions, O.M., Ward, A.M., Gubler, D.J., et al. (2015). Dengue subgenomic RNA binds TRIM25 to inhibit interferon expression for epidemiological fitness. Science *350*, 217–221. https://doi.org/10.1126/science.aab3369.
33. Whitehead, S.S., Falgout, B., Hanley, K.A., Blaney, J.E., Jr., Markoff, L., and Murphy, B.R. (2003). A live, attenuated dengue virus type 1 vaccine candidate with a 30-nucleotide deletion in the 3' untranslated region is highly attenuated and immunogenic in monkeys. J. Virol. *77*, 1653–1657. https://doi.org/10.1128/jvi.77.2.1653-1657.2003.
34. Pijlman, G.P., Funk, A., Kondratieva, N., Leung, J., Torres, S., van der Aa, L., Liu, W.J., Palmenberg, A.C., Shi, P.-Y., Hall, R.A., and Khromykh, A.A. (2008). A Highly Structured, Nuclease-Resistant, Noncoding RNA Produced by Flaviviruses Is Required for Pathogenicity. Cell Host Microbe *4*, 579–591. https://doi.org/10.1016/j.chom.2008.10.007.
35. Proutski, V., Gaunt, M.W., Gould, E.A., and Holmes, E.C. (1997). Secondary structure of the 3'-untranslated region of yellow fever virus: implications for virulence, attenuation and vaccine development. J. Gen. Virol. *78*, 1543–1549. https://doi.org/10.1099/0022-1317-78-7-1543.
36. Proutski, V., Gritsun, T.S., Gould, E.A., and Holmes, E.C. (1999). Biological consequences of deletions within the 3'-untranslated region of flaviviruses may be due to rearrangements of RNA secondary structure. Virus Res. *64*, 107–123. https://doi.org/10.1016/s0168-1702(99)00079-9.
37. Proutski, V., Gould, E.A., and Holmes, E.C. (1997). Secondary structure of the 3' untranslated region of flaviviruses: similarities and differences. Nucleic Acids Res. *25*, 1194–1202. https://doi.org/10.1093/nar/25.6.1194.
38. Bryant, J.E., Vasconcelos, P.F.C., Rijnbrand, R.C.A., Mutebi, J.P., Higgs, S., and Barrett, A.D.T. (2005). Size heterogeneity in the 3' noncoding region of South American isolates of yellow fever virus. J. Virol. *79*, 3807–3821. https://doi.org/10.1128/jvi.79.6.3807-3821.2005.
39. Funk, A., Truong, K., Nagasaki, T., Torres, S., Floden, N., Balmori Melian, E., Edmonds, J., Dong, H., Shi, P.Y., and Khromykh, A.A. (2010). RNA structures required for production of subgenomic flavivirus RNA. J. Virol. *84*, 11407–11417. https://doi.org/10.1128/jvi.01159-10.
40. Akiyama, B.M., Graham, M.E., O Donoghue, Z., Beckham, J.D., and Kieft, J.S. (2021). Three-dimensional structure of a flavivirus dumbbell RNA reveals molecular details of an RNA regulator of replication. Nucleic Acids Res. *49*, 7122–7138. https://doi.org/10.1093/nar/gkab462.
41. Silva, P.A.G.C., Pereira, C.F., Dalebout, T.J., Spaan, W.J.M., and Bredenbeek, P.J. (2010). An RNA pseudoknot is required for production of yellow fever virus subgenomic RNA by the host nuclease XRN1. J. Virol. *84*, 11395–11406. https://doi.org/10.1128/jvi.01047-10.
42. Bredenbeek, P.J., Kooi, E.A., Lindenbach, B., Huijkman, N., Rice, C.M., and Spaan, W.J.M. (2003). A stable full-length yellow fever virus cDNA clone and the role of conserved RNA elements in flavivirus replication. J. Gen. Virol. *84*, 1261–1268. https://doi.org/10.1099/vir.0.18860-0.
43. Durbin, A.P., Karron, R.A., Sun, W., Vaughn, D.W., Reynolds, M.J., Perreault, J.R., Thumar, B., Men, R., Lai, C.J., Elkins, W.R., et al. (2001). Attenuation and immunogenicity in humans of a live dengue virus type-4 vaccine candidate with a 30 nucleotide deletion in its 3'-untranslated region. Am. J. Trop. Med. Hyg. *65*, 405–413. https://doi.org/10.4269/ajtmh.2001.65.405.
44. Russell, K.L., Rupp, R.E., Morales-Ramirez, J.O., Diaz-Perez, C., Andrews, C.P., Lee, A.W., Finn, T.S., Cox, K.S., Falk Russell, A., Schaller, M.M., et al. (2022). A phase I randomized, double-blind, placebo-controlled study to evaluate the safety, tolerability, and immunogenicity of a live-attenuated quadrivalent dengue vaccine in flavivirus-naïve and flavivirus-experienced healthy adults. Hum. Vaccin. Immunother. *18*, 2046960. https://doi.org/10.1080/21645515.2022.2046960.
45. Shan, C., Muruato, A.E., Nunes, B.T.D., Luo, H., Xie, X., Medeiros, D.B.A., Wakamiya, M., Tesh, R.B., Barrett, A.D., Wang, T., et al. (2017). A live-attenuated Zika virus vaccine candidate induces sterilizing immunity in mouse models. Nat. Med. *23*, 763–767. https://doi.org/10.1038/nm.4322.
46. Zhang, Y.N., Li, N., Zhang, Q.Y., Liu, J., Zhan, S.L., Gao, L., Zeng, X.Y., Yu, F., Zhang, H.Q., Li, X.D., et al. (2021). Rational design of West Nile virus vaccine through large replacement of 3' UTR with internal poly(A). EMBO Mol. Med. *13*, e14108. https://doi.org/10.15252/emmm.202114108.
47. Lo, M.K., Tilgner, M., Bernard, K.A., and Shi, P.Y. (2003). Functional analysis of mosquito-borne flavivirus conserved sequence elements within 3' untranslated region of West Nile virus by use of a reporting replicon that differentiates between viral translation and RNA replication. J. Virol. *77*, 10004–10014. https://doi.org/10.1128/jvi.77.18.10004-10014.2003.
48. Montalvo Zurbia-Flores, G., Rollier, C.S., and Reyes-Sandoval, A. (2022). Re-thinking yellow fever vaccines: fighting old foes with new generation vaccines. Hum. Vaccin. Immunother. *18*, 1895644. https://doi.org/10.1080/21645515.2021.1895644.
49. Meier, K.C., Gardner, C.L., Khoretonenko, M.V., Klimstra, W.B., and Ryman, K.D. (2009). A mouse model for studying viscerotropic disease caused by yellow fever virus infection. PLoS Pathog. *5*, e1000614. https://doi.org/10.1371/journal.ppat.1000614.
50. Piras-Douce, F., Raynal, F., Raquin, A., Girerd-Chambaz, Y., Gautheron, S., Sanchez, M.E.N., Vangelisti, M., and Mantel, N. (2021). Next generation live-attenuated yellow fever vaccine candidate: Safety and immuno-efficacy in small animal models. Vaccine *39*, 1846–1856. https://doi.org/10.1016/j.vaccine.2021.02.033.
51. Medina-Magües, L.G., Mühe, J., Jasny, E., Medina-Magües, E.S., Roth, N., Lopera-Madrid, J., Salas-Quinchucua, C., Knuese, C., Petsch, B., and Osorio, J.E. (2023). Immunogenicity and protective activity of mRNA vaccine candidates against yellow fever virus in animal models. NPJ Vaccines *8*, 31. https://doi.org/10.1038/s41541-023-00629-7.
52. Thibodeaux, B.A., Garbino, N.C., Liss, N.M., Piper, J., Blair, C.D., and Roehrig, J.T. (2012). A small animal peripheral challenge model of yellow fever using interferon-receptor deficient mice and the 17D-204 vaccine strain. Vaccine *30*, 3180–3187. https://doi.org/10.1016/j.vaccine.2012.03.003.
53. Douam, F., and Ploss, A. (2018). Yellow Fever Virus: Knowledge Gaps Impeding the Fight Against an Old Foe. Trends Microbiol. *26*, 913–928. https://doi.org/10.1016/j.tim.2018.05.012.
54. Maciel, M., Jr., Kellathur, S.N., Chikhlikar, P., Dhalia, R., Sidney, J., Sette, A., August, T.J., and Marques, E.T.A., Jr. (2008). Comprehensive analysis of T cell epitope discovery strategies using 17DD yellow fever virus structural proteins and BALB/c (H2d) mice model. Virology *378*, 105–117. https://doi.org/10.1016/j.virol.2008.04.043.
55. Gaucher, D., Therrien, R., Kettaf, N., Angermann, B.R., Boucher, G., Filali-Mouhim, A., Moser, J.M., Mehta, R.S., Drake, D.R., 3rd, Castro, E., et al. (2008). Yellow fever vaccine induces integrated multilineage and polyfunctional immune responses. J. Exp. Med. *205*, 3119–3131. https://doi.org/10.1084/jem.20082292.
56. Muruato, A.E., Shan, C., Fontes-Garfias, C.R., Liu, Y., Cao, Z., Gao, Q., Weaver, S.C., and Shi, P.Y. (2019). Genetic stability of live-attenuated Zika vaccine candidates. Antivir. Res. *171*, 104596. https://doi.org/10.1016/j.antiviral.2019.104596.
57. Collins, N.D., and Barrett, A.D.T. (2017). Live Attenuated Yellow Fever 17D Vaccine: A Legacy Vaccine Still Controlling Outbreaks In Modern Day. Curr. Infect. Dis. Rep. *19*, 14. https://doi.org/10.1007/s11908-017-0566-9.
58. Porudominsky, R., and Gotuzzo, E.H. (2018). Yellow fever vaccine and risk of developing serious adverse events: a systematic review. Rev. Panam. Salud. Publica. *42*, e75. https://doi.org/10.26633/rpsp.2018.75.
59. Monath, T.P., Fowler, E., Johnson, C.T., Balser, J., Morin, M.J., Sisti, M., and Trent, D.W. (2011). An inactivated cell-culture vaccine against yellow fever. N. Engl. J. Med. *364*, 1326–1333. https://doi.org/10.1056/NEJMoa1009303.

60. Julander, J.G., Testori, M., Cheminay, C., and Volkmann, A. (2018). Immunogenicity and Protection After Vaccination With a Modified Vaccinia Virus Ankara-Vectored Yellow Fever Vaccine in the Hamster Model. Front. Immunol. *9*, 1756. https://doi.org/10.3389/fimmu.2018.01756.

61. Furtado, N.D., Raphael, L.d.M., Ribeiro, I.P., de Mello, I.S., Fernandes, D.R., Gómez, M.M., Dos Santos, A.A.C., Nogueira, M.D.S., de Castro, M.G., de Abreu, F.V.S., et al. (2022). Biological Characterization of Yellow Fever Viruses Isolated From Non-human Primates in Brazil With Distinct Genomic Landscapes. Front. Microbiol. *13*, 757084. https://doi.org/10.3389/fmicb.2022.757084.

62. Fitzgeorge, R., and Bradish, C.J. (1980). The *in vivo* differentiation of strains of yellow fever virus in mice. J. Gen. Virol. *46*, 1–13. https://doi.org/10.1099/0022-1317-46-1-1.

63. Monath, T.P., Lee, C.K., Julander, J.G., Brown, A., Beasley, D.W., Watts, D.M., Hayman, E., Guertin, P., Makowiecki, J., Crowell, J., et al. (2010). Inactivated yellow fever 17D vaccine: development and nonclinical safety, immunogenicity and protective activity. Vaccine *28*, 3827–3840. https://doi.org/10.1016/j.vaccine.2010.03.023.

64. Wang, H.J., Guo, Y., He, M.J., Liu, Z.Y., Ye, Q., Huang, X.Y., Deng, Y.Q., Li, X.F., and Qin, C.F. (2022). Development of a Bicistronic Yellow Fever Live Attenuated Vaccine with Reduced Neurovirulence and Viscerotropism. Microbiol. Spectr. *10*, e0224622. https://doi.org/10.1128/spectrum.02246-22.

65. Shi, P.Y., Tilgner, M., Lo, M.K., Kent, K.A., and Bernard, K.A. (2002). Infectious cDNA clone of the epidemic west nile virus from New York City. J. Virol. *76*, 5847–5856. https://doi.org/10.1128/jvi.76.12.5847-5856.2002.

66. Shan, C., Xie, X., Muruato, A.E., Rossi, S.L., Roundy, C.M., Azar, S.R., Yang, Y., Tesh, R.B., Bourne, N., Barrett, A.D., et al. (2016). An Infectious cDNA Clone of Zika Virus to Study Viral Virulence, Mosquito Transmission, and Antiviral Inhibitors. Cell Host Microbe *19*, 891–900. https://doi.org/10.1016/j.chom.2016.05.004.

67. Kümmerer, B.M. (2018). Establishment and Application of Flavivirus Replicons. Adv. Exp. Med. Biol. *1062*, 165–173. https://doi.org/10.1007/978-981-10-8727-1_12.

STAR★METHODS

KEY RESOURCES TABLE

REAGENT or RESOURCE	SOURCE	IDENTIFIER
Antibodies		
Pan-flavivirus E-specific mouse monoclonal antibody hybridoma D1-4G2-4-15	ATCC	ATCC HB-112; RRID: AB_2940755
Alexa Fluor 488 Goat anti-Mouse IgG (H + L)	Invitrogen	Cat# A-11029; RRID: AB_2534088
HRP-conjugated Goat Anti-Mouse IgG	Proteintech	Cat# SA00001-1; RRID: AB_2722565
Bacterial and virus strains		
E. coli Top10	Beyotime	Cat# D1087M
YF17D (Strain 17D RKI, GenBank number JN628279)	This paper	N/A
YF17D-mScarlet	This paper	N/A
YF17D-Δ77	This paper	N/A
YF17D-Δ50	This paper	N/A
YF17D-Δ30	This paper	N/A
YF17D-Δ20	This paper	N/A
YF17D-Δ10	This paper	N/A
YF17D-Δ77-mScarlet	This paper	N/A
YF17D-Δ50-mScarlet	This paper	N/A
YF17D-Δ30-mScarlet	This paper	N/A
YF17D-Δ20-mScarlet	This paper	N/A
YF17D-Δ10-mScarlet	This paper	N/A
YFV-Asibi (GenBank number AY640589.1)	This paper	N/A
Chemicals, peptides, and recombinant proteins		
YFV E peptides (E60-68, E330-338, E133-147)	Maciel et al.[54]	Maciel et al.[54]
IFN-γ, human	Genscript	Cat# Z02986
IFN-β, human	Genscript	Cat# Z03109
Restriction endonucleases	New England Biolabs	N/A
Hoechst	Invitrogen	Cat# MP 21486
Critical commercial assays		
mMESSAGE mMACHINE T7 Transcription Kit	Ambion	Cat# AM1344
PrimeSTAR® Max DNA Polymerase	TAKARA	Cat# R045A
Q5 Site-Directed Mutagenesis Kit	New England Biolabs	Cat# E0554
Electroporation Solution	Mirus Bio	Cat# MIR50117
Nano-Glo Luciferase Assay System	Promega	Cat# N1110
Cytotoxicity LDH Assay Kit -WST®	DOJINDO	Cat# CK12
QIAamp Viral RNA Kit	Qiagen	Cat# 52906
SuperScript III one-step RT-PCR kits	Invitrogen	Cat# 12574030
Mouse IFN-γ ELISpot kit	MABTECH	Cat# 3321-4APT
HiScript II One Step qRT-PCR Probe Kit	Vazyme	Cat# Q222-01
Experimental models: Cell lines		
Hamster: BHK-21 cells	ATCC	ATCC CCL10
African green monkey: Vero cells	ATCC	ATCC CCL81

(*Continued on next page*)

Continued

REAGENT or RESOURCE	SOURCE	IDENTIFIER
Aedes albopictus: C6/36 cells	ATCC	ATCC CRL-1660
Experimental models: Organisms/strains		
Mouse: BALB/c	Beijing Vital River	N/A
Mouse: A129: IFNαβR−/−	Beijing Vital River	N/A
Mouse: AG129: IFNαβγR$^{-/-}$	Beijing Vital River	N/A
Oligonucleotides		
Primer for qRT-PCR: Forward: 5′-gcacggatgtaacagactgaaga-3′	This paper	N/A
Primer for qRT-PCR: Reverse: 5′-ccaggccgaacctgtcat-3′	This paper	N/A
Probe for qRT-PCR: 6-FAM-cgactgtgtggtccggcccatc-BHQ1	This paper	N/A
Primer for RT-PCR1: Forward: 5′-AGTAAATCCTGTGTGCTAATTG-3′	This paper	N/A
Primer for RT-PCR1: Reverse: 5′-TAGCGGCTATGCTAGCTGGAT-3′	This paper	N/A
Primer for RT-PCR2: Forward: 5′-TCACGGCCTGGACGTGAAATT-3′	This paper	N/A
Primer for RT-PCR2: Reverse: 5′-AGTGGTTTTGTGTTTGTCATC-3′	This paper	N/A
Recombinant DNA		
pFL-17D	This paper	N/A
pFL-Asibi	This paper	N/A
pFL-17D-mScarlet	This paper	N/A
p17D-Rep.	This paper	N/A
pFL-17D-Δ10/20/30/50/77	This paper	N/A
pFL-17D-Δ10/20/30/50/77-mScarlet	This paper	N/A
p17D-Δ10/20/30/50/77-Rep.	This paper	N/A
p17D-Rep-NS5ΔGDD	This paper	N/A
Software and algorithms		
GraphPad Prism (version 8.3.0)	GraphPad Software	https://www.graphpad.com/
Adobe Illustrator (version 24.1.3)	Adobe	https://www.adobe.com/
SnapGene	SnapGene	https://www.snapgene.com/
Evos Analysis	Thermo Fisher	N/A
Other		
Evos M7000	Thermo Fisher	N/A
96-Well Clear Flat Bottom Black Polystyrene Microplate	Corning	Cat# 3603
Gene Pulser Xcell	Bio-rad	Cat# 1652660
Electroporation Cuvette	Bio-rad	Cat# 1652081
AID ELISPOT Reader Classic	AID	N/A

EXPERIMENTAL MODEL AND STUDY PARTICIPANT DETAILS

Cells, viruses and antibodies

Vero and BHK-21 cells were cultured in high-glucose Dulbecco modified Eagle medium (DMEM) supplemented with 10% (v/v) fetal bovine serum (FBS), 100 units/ml penicillin and 100 μg/mL streptomycin (1% PS) and incubated at 37°C with 5% CO2. *Aedes albopictus* C6/36 cells were maintained in RPMI 1640 medium supplemented with 10% FBS, 1% PS and 250 mg/ml amphotericin B, and incubated at 28°C with 5%

CO2. All viruses (YF17D,17D-mutant viruses, YF17D-mScarlet, 17D-mutant-mScarlet and YFV-Asibi) used in this study were generated from infectious cDNA clones. The pan-flavivirus E-specific mouse monoclonal antibody 4G2 was obtained from the ascites of hybridoma. Generally, 10^6 commercial hybridoma D1-4G2-4-15 (ATCC HB-112) were injected intraperitoneally to BALB/c mice which were sensitized with adjuvant for 14 days in advance. The ascites fluid was taken one week later and stored at −80°C after centrifugation until use. Goat anti-Mouse IgG (H + L) conjugated with Alexa Fluor 488 (Invitogen) and HRP-conjugated Goat Anti-Mouse IgG (Proteintech) were used as secondary antibody. All cell lines are tested negative for mycoplasma.

Bacterial strains

We used *E.coli* Top 10 strain for plasmids transformation and propagation. *E. coli* was grown in LB medium supplemented with 100 μg per milliliter of ampicillin sodium.

Animals

We purchased the female, 6–8-week-old BALB/c mice from Beijing Vital River Laboratory Animal Technology Co., Ltd. We bred A129 and AG129 mice at the Laboratory Animal Center of the Wuhan Institute of Virology, Chinese Academy of Sciences. All the mice were cared following the recommendations of National Institutes of Health Guidelines for the Care and Use of Experimental Animals. Studies related to virus infection were performed in Animal Biosafety Level 2 (ABSL-2) and National Biosafety Laboratory Level 3 facility at Wuhan Institute of Virology under a protocol approved by the Laboratory Animal Ethics Committee of Wuhan Institute of Virology, Chinese Academy of Sciences (WIVA42202304).

METHOD DETAILS

cDNA synthesis and plasmid construction

cDNA fragments of YF17D (Strain 17D RKI, GenBank number JN628279) and YFV-Asibi (GenBank number AY640589) covering the complete genome were synthesized from GenScript company. The full-length genomic cDNA of YF17D and YFV-Asibi were constructed into a low-copy number plasmid pACYC177 (New England Biolabs) using standard molecular cloning approaches, as previously described for constructing WNV[65] and ZIKV[66] infectious clones. Briefly, two overlap fragments covering the complete genome were amplified from synthesized subclones via PCR with primer pairs NotI-T7-F1/NheI-17D/Asibi5469-R1, NheI-17D/Asibi5453-F2/AsisI-HDVr-R. Purified PCR fragments were used to assemble full-length genomic cDNA using the NEBuilder HiFi DNA Assembly kit (E5520) according to the manufacturer's instruction. In the final infectious clone (pFL-17D and pFL-Asibi) the T7 promoter and a hepatitis delta virus ribozyme (HDVr) sequence were introduced upstream of the 5′UTR and downstream of the 3′UTR respectively to initiate *in vitro* transcription and generate an authentic 3′ end of the RNA transcript. The *Nano* luciferase (Nluc) replicon plasmid was constructed based on pFL-17D. Standard overlap PCR was performed to amplify the DNA fragment (5′ UTR-C25-Nluc-2A-E24 in-frame fused with the ORF) between unique restriction enzyme sites NotI and MluI, in which most partial of the structural sequences (YF17D genome nt194-2380) was replaced by Nluc gene and foot-and-mouth disease virus (FMDV) 2A sequences (Nluc-2A). The preserved sequences of C protein (N-terminal 25 amino acids) are flavivirus conserved cyclization sequences required for viral RNA replication, and the C-terminal 24 amino acids in the E protein (E24) serve as a signal peptide for proper translocation of NS1 into the endoplasmic reticulum (ER) lumen.[67] The purified PCR fragment was cloned into pFL-17D through the NotI and MluI sites, resulting in the production of p17D-Rep. Similar strategy was used to construct pFL-17D-mScarlet. Briefly, a fragment (C25-mScarlet-2A) was engineered between the 5′ UTR and ORF in pFL-17D. All deletions in 3′UTR were individually introduced into the pFL-17D, pFL-17D-mScarlet, and p17D-Rep through AsisI and ClaI. As a control, the conserved functional motif GDD[67] (corresponding to residues Gly666, Asp667, and Asp668 in YF17D NS5) of YF17D polymerase was mutated to Ala (G666A-D667A-D668A) using Q5® Site-Directed Mutagenesis Kit (NEB, E0554), resulting in plasmid p17D-Rep-NS5ΔGDD. Primer sequences are available upon request. All the constructs were verified by Sanger DNA sequencing.

RNA transcription, transfection, and virus rescue

All validated plasmids (infectious clones and replicons) were amplified in *E.coli* Top10 and extracted using QIAGEN plasmid plus MAXI kit (12963) according to the manufacturer's instructions. Ten microgram of each plasmid was linearized with AsisI at 37°C for 2 hours and followed by purification with phenol-chloroform and chloroform. Linearized plasmid in the aqueous phase was precipitated with ethanol and was re-dissolved in RNase-free water. Infectious and replicon RNAs were *in vitro* transcribed using mMESSAGE mMACHINE T7 Transcription Kit (Ambion, AM1344) as described previously for ZIKV.[66] In general, 1-2 μg purified linear plasmid was added as template in a 20 μl reaction system, followed by 2 hours incubation at 37°C, after that 1 μl DNase was added to digest the DNA template. After precipitating with lithium chloride and washing with 70% ethanol, the RNA pellet was re-suspended in RNase-free water and stored at -80°C in aliquots. Ten micrograms of infectious RNA (FL-17D and FL-17D-mutants) was added to a 4-mm cuvette containing 0.8 ml of Vero cells (8×10^6) in Electroporation Solutions (Mirus, MIR50117). Electroporation was conducted at settings of 0.45 kV and 25 μF, pulsing three times, with 3-second intervals using a GenePulser apparatus (Bio-Rad). Infectious RNA of FL-Asibi and FL-17D-mCherry and Replicon RNAs (17D-Rep, 17D-mutants-Rep and 17D-Rep-NS5ΔGDD) were electroporated into BHK-21 cells at 0.85 kV and the other conditions were the same as described for Vero cells. The transfected cells were diluted with fresh culture medium and then plated or returned to flasks and were incubated at 37°C with 5% CO_2. After 24 h of transfection the culture medium of the infectious RNA transfected cells was replaced with fresh culture medium. After 8-10 days of

incubation, viruses (YF17D, YFV-Asibi, YF17D-mutants, YF17D-mScarlet, YF17D-mutant-mScarlet) in culture medium were harvested as virus stock (P0 generation) and stored at -80°C in aliquots. The replicon RNA transfected cells were treated as described below. The operations of YFV-Asibi were carried out in National Biosafety Laboratory level 3 facility.

Virus titration and growth kinetics

For viral titration, the viral stocks and other viral samples were 10-fold serially diluted in DMEM, 100 μl of each dilution was taken to infect the BHK-21 monolayer cells in 24-well plates (The cells were plated at 1.5×10^5 cells per well 1 day in advance) and were incubated at 37°C for 1 h before the semi-solid medium (0.8% methylcellulose was added in culture medium) was covered. After 5-7 days of incubation, cells are fixed with 3.7% paraformaldehyde prior to 0.5 % crystal violet staining. Plaque-forming units (PFU)/mL were calculated as viral titres.

Immunostaining focus assay was also used for P0 viral titration. Vero cells in 24-well plate (The cells were plated at 2.0×10^5 cells per well 1 day in advance) were infected with diluted viral samples as described in viral titration. Six days after incubation the cells were fixed with formaldehyde-acetone (1:1) solution for 15 minutes and washed with PBS 3 times and then blocked with 5% BSA in PBS, followed by administrating 4G2 (1:500) as the primary antibody and HRP-conjugated Goat Anti-Mouse IgG (1:2000) as the secondary antibody and finally the substrate was added to make the spots visible.

To test viral growth kinetics, sub confluent Vero cells and C6/36 cells in 24-well plates (Vero or C6/36 cells were plated at 1.5×10^5 or 4×10^5 cells per well 1 day in advance) were infected with P0 viruses at an multiplicity of infection (MOI) of 0.05. After 1h of incubation (37°C for Vero cells and 28°C for C6/36 cells), the cell monolayers were washed three times with PBS before 0.5 ml of culture medium was added to each well. Cell culture fluids in triplicate wells were harvested every 24h to determine viral titres.

Indirect immunofluorescence assays (IFA)

The expression of YF17D E protein in Vero cells transfected with infectious RNAs were tested by IFA. At indicated time points, cells grown in a cell crawler were fixed for 15 min at −20°C with 100% methanol and then saturated for 1h with a 1% FBS-0.05% Tween20-PBS buffer, followed by immunostaining with anti-E protein monoclonal antibody 4G2 (1:500) and were incubated with Goat anti-Mouse IgG (H+L) (Alexa Fluor™ 488) in dark for 1h. Nuclei were stained with Hoechst (Invitrogen, MP 21486). The images were captured with EVOS at ×400 magnification.

Luciferase assay

Viral RNA synthesis kinetics were determined by detecting luciferase signaling in replicon RNA transfected cells. Briefly, BHK-21 cells transfected with YF17D or mutant-17D replicon RNA were seeded into 24-well plates at 1.3×10^5 cells per well. At indicated time points, cells in triplicate wells were lysed for 10 min with cell lysis buffer (Promega, E2661) at room temperature. The lysate was collected and store at -80°C until detected with Nano-Glo® Luciferase Assay System (Promega, N1110).

LDH assay

Vero cells were plated at 15,000/well in 96-well plates and infected with YF17D or mutant viruses at an MOI of 0.05. Eight days after infection, LDH release in culture medium was measured with Cytotoxicity LDH Assay Kit -WST® (DOJINDO, CK12) according to the manufacturer's instructions. The damaged cells % was calculated using the formula provided by the manufacturer.

Interferon (IFN) inhibition assay

Vero cells were seeded in black 96-well plate (1.5×10^4 cells per well) one day before interferon treatment and viral infection. YF17D-mScarlet and 17D-mutant-mScarlet infected Vero cells at an MOI of 0.1 in the presence of different concentrations of IFN-β (3125, 1563, 781, 391 and 195 pg/ml) or IFN-γ (126, 42, 14, 4.7 and 1.6 ng/ml). After 48 h of infection, the red fluorescent signal was captured by a fluorescence microscopy EVOS and was quantified by the Evos Analysis.

Stability of mutant virus, RNA extraction, and RT-PCR

YF17D-Δ77 was successively passaged in Vero cells to examine the stability of the Δ77 deletion in 3′ UTR. Briefly, P0 virus (100 μl) was added into sub confluent Vero cells in T25 flasks, after 5 days of incubation, the culture fluids were harvested as P1 viruses and 100 μl of P1 viruses were taken to infect new Vero cells in T25 flasks. After 20 rounds of passaging, RNAs of P20 YF17D-Δ77 were extracted using QIAamp Viral RNA Kit (Qiagen, 52906), full-length viral cDNA was amplified by RT-PCR using SuperScript III one-step RT-PCR kits (Invitrogen, 12574030) and subjected to Sanger sequence. Three independent trials were performed simultaneously.

Safety testing in A129 and AG129 mice

To test the tissue tropism of the mutant viruses, three- to four-week-old mixed sex IFNαβR−/− A129 mice were s.c. injected with 10^4 PFU of YF17D or mutant viruses in 100 μl PBS. Five mice in one group were euthanized on day 2, 4, and 6 post-infection, the drain lymph nodes, livers, spleens, bone marrows and brains of the mice were collected for infectious virus detection after weighing, homogenization and clarification. Blood was collected 2-5 days after infection to measure viremia. To test the pathogenicity of the mutant viruses in AG129 mice (IFNαβγR−/−), six- to eight-week-old mixed sex mice were infected with lethal dose (10^4 PFU) of YF17D or the same dose of mutant viruses via the i.p. route.

The infected mice (n = 9) were monitored daily for survival, viremia, and body weight changes. The other animals were used to analysis viral tissue tropism by the same method as described in A129 mice.

Immunization and challenge in A129 mice

To evaluate the immunogenicity of mutant viruses, three- to four-week-old mixed sex IFNαβR−/− A129 mice were s.c. injected with 10^4 PFU (high dose) and 10 PFU (low dose) of YF17D, mutant viruses or P20-2 YF17D-Δ77 in 100 μl PBS, mock-immunized mice were given equal volumes of PBS. On day 28 post-immunization, mice were bled for neutralization antibodies (nAbs) testing. On day 30 post-immunization, mice were challenged with 10^6 PFU of YFV-Asibi via i.p. route. On day 2 post-challenge, the mice were bled for viremia measurement. On day 6 post-challenge, the partial mice (n = 5 per group) were euthanized, the livers, spleens, bone marrows, and brains of mice were harvested for viral RNA copies detection by quantitative real-time reverse transcriptase PCR (qRT-PCR). The other challenged mice (n = 5 per group) were continuously observed for 14 days to monitor progression of disease and body weight changes. Three groups of mice (immunized with high dose of YF17D or YF17D-Δ77 and mock-immunized with PBS) were monitored for 1 year and were bled at 4, 8, 16, 32, 50 weeks post-immunization for nAbs detection. Two days after the last blood collection, mice were challenged with 10^6 PFU of YFV-Asibi via i.p. route and then subjected to 14 days of health monitoring.

Neutralizing antibody test

Neutralizing ability of mouse sera was assessed by two methods: the 50% reporter signal reduction neutralization test (RRNT50) with YF17D-mScarlet and the 50% plaque reduction neutralization test (PRNT50) with YFV-Asibi. Three-fold serially diluted mice sera (1:50,1:150,...,1:12150) were co-incubated with YF17D-mScarlet at 37°C for 1 h. The mixture of sera-virus was taken to infect confluent Vero cells in black 96-well plates (The cells were plated at 2.0×10^4 cells per well 1 day in advance). After 48 h incubation at 37°C, the red fluorescence-positive cells were visualized and quantified using a fluorescence microscopy EVOS. The red fluorescence-positive cells in serum-treated wells were normalized to those of control (mouse serum-free) wells. The RRNT50 value was calculated using a four-parameter sigmoidal (logistic) model in the software GraphPad Prism 8.

The ability of mouse sera to neutralize YFV-Asibi was evaluated by PRNT50. Heat-inactivated immune sera were 2-fold serially diluted in DMEM containing 2% FBS and 1% penicillin/streptomycin, from 1:20 to 1:640. The diluted sera were co-incubated with 50 PFU of YFV-Asibi at 37°C for 1h. The mixture of sera-virus was taken to infect BHK-21 monolayer cells in 24-well plates (the cells were plated at 1.5×10^5 cells per well 1 day in advance). After 1h of incubation at 37°C, the infected material was replaced with semi-solid medium. After 4 days of incubation at 37°C with 5% CO_2, the cells were fixed with 3.7% paraformaldehyde prior to 0.5% crystal violet staining. The plaques in serum-treated wells were normalized to those of control (mouse serum-free) wells. The PRNT50 value was calculated using the same algorithm as for RRNT50 value.

Enzyme-linked immunospot (ELISpot) assay

ELISpot assay was performed to assess cellular immune responses using Mouse IFN-γ ELISpot kit (MABTECH, 3321-4APT) according to the manufacturer's recommendations. Briefly, splenocytes were isolated from six- to eight-week-old female BALB/c ($H2^d$) mice that immunized via I.C. route with 10^4 PFU of YF17D or mutant viruses. After 8 days or 6 months of immunization, fresh splenocytes were plated at 5×10^5 per well in pre-coated ELISpot plate. Three YFV E peptides, E60-68 (CYNAVLTHV), E330-338 (CRIPVIVAD) and E133-147 (TKIQYVIRAQLHVGA),[54] were added at 100 ng per well to stimulate virus-specific T cell activation and IFN-γ secretion. Equal volumes of solvent and a mixture of phorbol 12-myristate 13-acetate (PMA) and ionomycin (Dakewe) were used as the negative and positive stimulus, respectively. After incubation at 37°C, 5% CO2 for 24 h, the plates were washed and were incubated with detection antibody for 2 h and followed by incubation with streptavidin-ALP for 1 h. Distinct spots emerged 5-10 minutes after administrating the substrate solution. The spots were scanned and counted using AID ELISPOT READER (Germany), each spot represents an activated functional T cell. Finally, IFN-γ spot-forming cells (SFC) per million splenocytes was calculated.

qRT-PCR

RNAs were extracted from clarified mouse tissue homogenate using QIAamp Viral RNA Kit (Qiagen, 52906). Viral RNA in mouse tissues was quantified by qRT-PCR using the HiScript II One Step qRT-PCR Probe Kit (Vazyme, Q222-01). YFV-specific primers (forward primer: 5′-gcacggatgtaacagactgaaga-3′, reverse primer: 5′-ccaggccgaacctgtcat-3′) and probe (6-FAM-cgactgtgtggtccggcccatc-BHQ1) were used in the recommended reaction system. Standard RT-PCR program suggested by the manufacturer was performed on a CFX96 Real-Time System (Bio-Rad). RNA standards were prepared by *in vitro* transcription and were 10-fold serially diluted (10^1-10^9 copies) to as the qRT-PCR template to construct a standard curve.

QUANTIFICATION AND STATISTICAL ANALYSIS

GraphPad Prism 8.0 software were used to statistical analysis. Quantitative data from three independent experiments were presented as mean ± standard deviations. The significance was calculated using one- or two-way analysis of variance (ANOVA) in more than two groups comparison. The significance of Kaplan-Meier survival curves was assessed by the Log-rank test. Statistical significance was represented as: * $P < 0.05$, ** $P < 0.01$, *** $P < 0.001$, **** $P < 0.0001$, ns = not significant.